Mapping of Soil Physical Properties for Predicting Preferential Flow at the Field Scale

Case Study: The Pesticide Leaching Monitoring Field at Silstrup, Denmark

MSc thesis

Discipline: Hydrology, Hydrogeology and Soils

Student: Luong Nhat Minh
Supervisor: Lis Wollesen de Jonge
Co-supervisor: Bo Vangsø Iversen
Mathieu Lamandé

Orsay, September 2011

Acknowledgements

In first place, I want to give my deepest thanks to my supervisor, Lis Wollesen de Jonge from Aarhus University, who gave me chance to do this study, my co-supervisor Bo Vangsø Iversen and Mathieu Lamandé for their guidance and precious advices all along the duration of my internship

I also want to thank Professor Per Moldrup from Department of Environmental Engineering at Aalborg University who gave me a lot of AWeSOMe ideas and recommendations to this thesis.

Abstract

The risk of groundwater contamination by pesticides, nutrients, trace metals, and pathogens has been known to occur not only in the areas where the hydraulic conductivity is elevated, such as coarse-grained sandy soils with a low organic matter content, but also in structured soils where preferential flow may be a governing factor. To protect groundwater resources it is necessary to have a risk assessment map of the areas which are a highly prone to contamination. This study aims to develop a tool combining prediction (by pedo-transfer functions) and mapping to identify areas within a single field scale that are highly susceptible to the development of macropore flow. In this study, different approaches such as texture analysis, air transport parameters, water transport soils parameters and leaching experiment using tritium as a tracer were employed These methods linked by simple correlation or pedo-transfer-functions (PTFs), combined with smart field-scale mapping of the parameters can become a new, valuable tool for assessment of chemical leaching risks. The combined mapping and PTF tool is suggested as a part of a decision platform for management of pesticides application on the field.

Key words: preferential flow, macropore, breakthrough curves, transfer function, Pedo-transfer functions

Table of content

List of the Appendices

1 Introduction

Soils are among the most complex systems found in the nature with physical, chemical, and biological components and processes taking place simultaneously (Ritz 2008). Due to this reason, there is no mathematic equation that can describe exactly the movement of water in soils. Properties of soil are the principal factor controlling the fate of contaminants leaching to the ground water. Contaminants reach groundwater table by moving with percolating water through the soil pores. Many contaminants are degradable or can be adsorbed to the surfaces of soil particles, while others are very persistent. Microorganisms present in soils may break down contaminants into either harmless or even more harmful compounds before reaching the groundwater (Hornsby 2003).

In Denmark, an increase in variety of pesticides and pesticide degradation products in drinking water wells has been detected over the past decades. According to Thorling et al., (2010), pesticides have been detected in 53% of all monitored screens and in 61% of the screens placed in the upper groundwater. As the result, several drinking water wells were shut down during the period from 1994 - 2001. It is presumed that approximately 100-150 drinking water wells are closed per year (GEUS, 2009). After detection of increased presence of pesticides and degradation products in monitoring screens in the period between 1993-1998 reported by the Danish Groundwater Monitoring Program (GRUMO) (GEUS, 2000), the Danish Pesticide Leaching Assessment Program (PLAP) was established in 1998 with the main purpose of monitoring the leaching of pesticides and reducing their concentration to acceptable concentration of 0.1µg/L (EU frame directive for water quality). When established, PLAP was consisted of six test sites located at different places all over the country, representing the dominant soil types and climatic conditions present in Denmark. Based on the lysimeter measurements coupled with hydro-geological investigation and laboratory studies, more than 40 types of different categories of pesticides have been recognized and evaluated. More information about PLAP can be consulted at www. http://pesticidvarsling.dk

The risk of groundwater contamination by pesticides, nutrients, trace metals, and pathogens depends on numerous factors, including the chemical properties of the pollutant, climatic conditions, hydrogeology, types, and structure of soil. The risk of leaching of pesticides has been known to occur not only in the areas where the hydraulic conductivity is elevated, such as coarse-grained sandy soils with a low organic matter content, but also in structured soils (Flurry et al.,1996) where preferential flow may be a governing factor.

Preferential flow is described as a process where water and solutes move along certain pathways while bypassing a large fraction of the porous matrix (Hendrickx and Flury, 2001). Preferential flow includes e.g. flow in structural macropores (Jarvis et al., 2007), finger flow caused by wetting front instabilities (Hillel, 1987) or water-repellent soil (Thomas et al., 1973; Doerr et al., 2000), and entrapped air (Cislerova et al., 1988). Through these pathways, water and solutes can propagate much faster to reach the groundwater. Moreover, preferential flow can be formed by the fracture of parental rock, earthworm burrows, and channels of decayed roots or drying cracks in swelling clay soils (Beven and German, 1982; Gerke et al., 2006). Preferential flow and transport processes are probably the most challenging phenomena in terms of hampering accurate predictions of contaminant transport in soils and fracture rocks (Simunek et al., 2003).

Preferential transport is a governing process responsible for the leaching of phosphorus in structured soils due to the macropore flow (Ulén and Person, 1999; de Jonge et al., 2004; Kleinman et al., 2005). Typically, pesticide loss due to the macropore flow is less than 1% of the applied dose but sometimes goes up to 5% (Jarvis, 2007). Preferential flow contributes very significantly to underground water recharge, an average of 75% of total recharge in a case of fractured granites (Sukhija et al., 2003), but on the other hand, it can induce risk of contamination.

1.1 Mechanisms behind and prediction of the risk of for preferential flow

The importance of preferential flow, including macropore flow, was recognized very early by Lawes et al., (1892). However, until the beginning of the 1970's with the new experimental observations of rapid non-equilibrium flow of water in macropore, this topic attracted attention of numerous scientists focusing on all aspects of macropore flow in soils.

Figure 1 shows the mechanism of macropore flow. This mechanism was well described by Jarvis (2007) by imagining a block of soil wetting up towards saturation during infiltration. At the point A, the macropores are air-filled, only the surface is wet and the water flow is restricted only to the soils matrix. When soil moisture content increases to the pressure potential B, the non-equilibrium matrix flow and macropore flow begins to develop and water starts to flow through the macropores. At the point C, the soil is not totally saturated but water is occupying all the interconnected macropores and starts flowing continuously. Therefore, when the block of soil is completely saturated, the macropores are responsible for the majority of the water transport, following Poiseuille’s law. According to capillarity, the soil matric potential between -10 cm and -6 cm corresponds to an equivalent cylindrical pore diameter of 0.3-0.5 mm which can be classified as macropores (Beven and German, 1982; Jarvis et al., 2007).

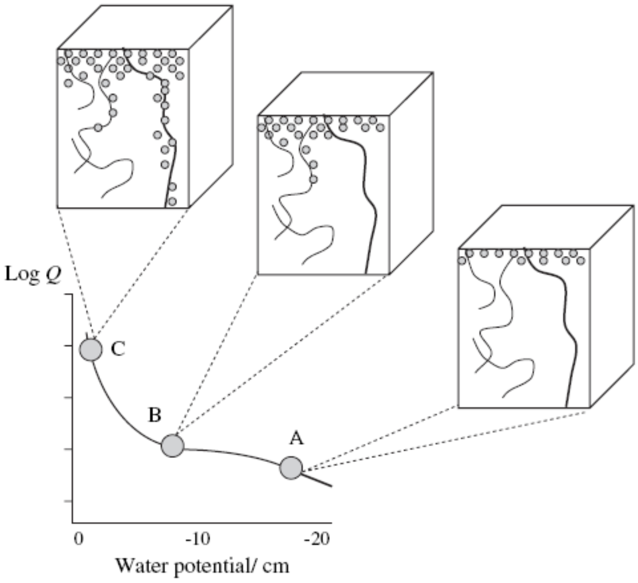

Figure 1 : Mechanism of macropore flow in soil under differing infiltration rates and generation of non-equilibrium flow in macropores. For the explanation of A, B, and C see text (Jarvis et al., 2007).

Based on the concept explained above, Iversen et al., (2011) pointed out that the difference of logarithm of saturated hydraulic conductivity, log(*Ks*), and logarithm of unsaturated hydraulic conductivity at matric potential of -10 cm (log(*k[-10]*)) [Eq. 1] can be regarded as an indirect estimation of the potential of water transport through soil macropores. A large value of log(k_{jump}) is often observed in loamy soils (Figure 2a) while a small value of log(k_{jump}) occurs in sandy soils where the pore sizes are homogenous and matrix flow is dominant (Figure2b) (Jarvis et al,2007; Iversen et al.,2011).

$$\mathrm{Log}(k_{jump}) = \mathrm{Log}(K_s) - \mathrm{Log}\,(k[-10]) \qquad [1.1].$$

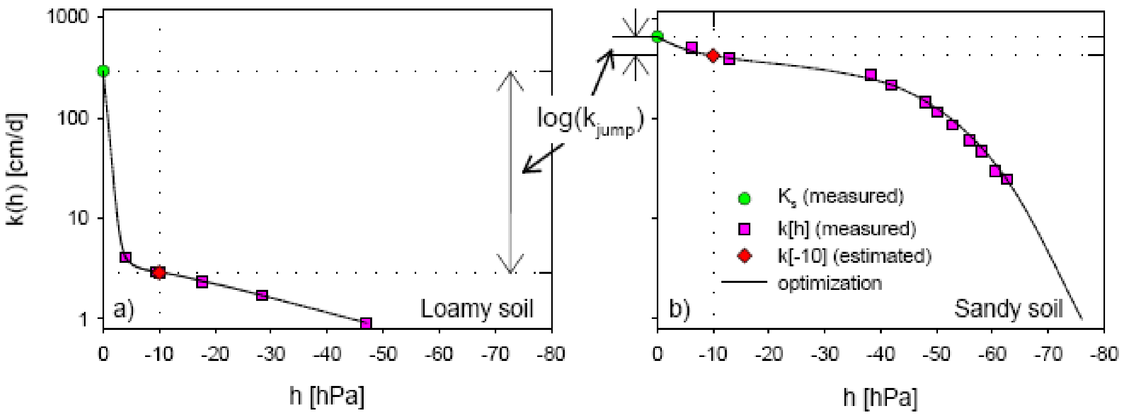

Figure 2 : Example of a measurement of the saturated hydraulic conductivity Ks and unsaturated hydraulic conductivity k[h] in a) a loamy soil , b) sandy soil (Iversen et al.,2011).

Moreover, in the study of Iversen et al. (2011), the map of prediction of risk of macropore flow (Figure 3) for the top soil (depth of 0-25cm) all over the Denmark was created, based on the Danish soils survey data of 45000 point samples (Greve et al., 2007). A pedo-transfer function (PTF) using neural network was used in order to predict the value of Ks and k[-10]. The risk of macropore flow was shown to be more important in the south-eastern part of Denmark with the high clay content in soils, whereas the sandy soils in the western part of the country are less susceptible to induce macropore flow (Figure 3).

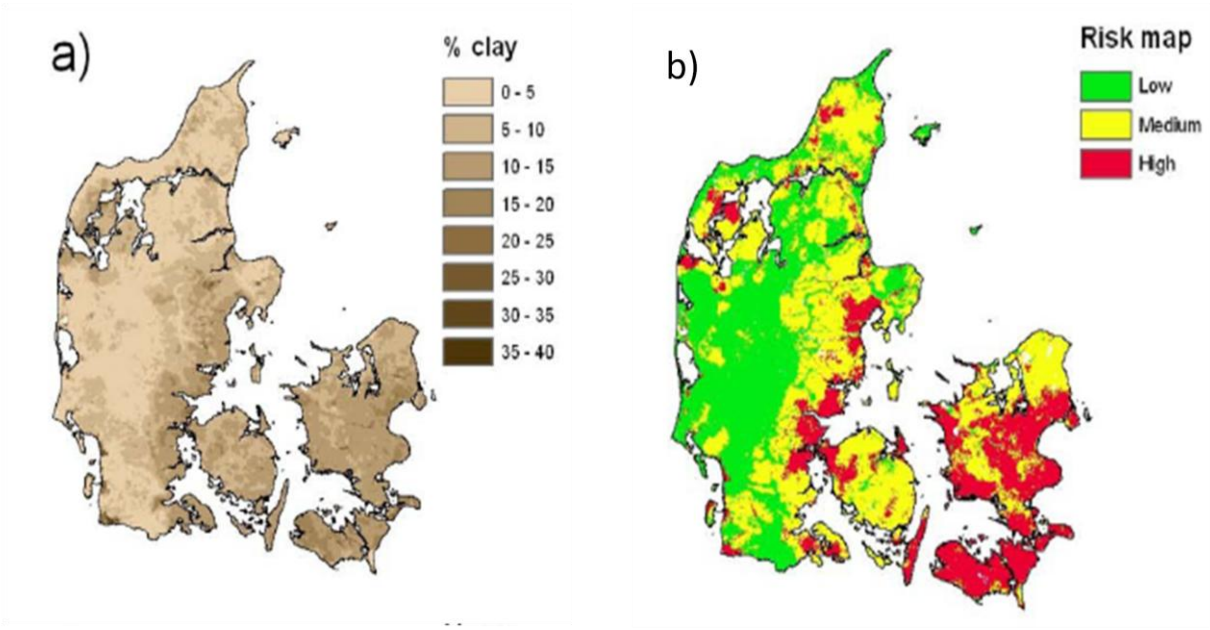

Figure 3 Maps showing a) clay content, b) risk of macropore flow

The preferential flow can also be investigated by conducting the leaching experiments on undisturbed soil column controlled by specific initial and steady-state hydraulic boundary condition to which conservative tracer was applied (such as Tritium, Bromide, or Chlorid…). The plot of the concentration of tracer in effluent normalized in regard to the amount of tracer vs. times is called the tracer breakthrough curve (BTC). The characteristics of the BTC, such as positive skewness, long tailing or early and high peak of concentration are representative of the degree of preferential flow. Many approaches have been employed to characterize the degree of the preferential flow. Comegna et al. (1999) and Stagnitti et al. (2000) used the arrival time of the median or the peak concentration relative to one pore volume as an indicator of preferential transport. Others investigated the temporal moments of the BTC (Jacobsen et al., 1992; Leij and Dane, 1992; Stagnitti et al., 2000) or used the non-parametric BTC shape such as 5% of the first tracer arrival time (Knudby et al., 2005; Kloestel et al., 2011*)*. Even if the model fits the observed data very well, the predicting of BTC is sensitive to the choice of deconvolution approach (Kloestel et al., 2011).

1.2 Project objectives

Based on the above observations from the literature, this study aims to develop a tool combining prediction (by pedo-transfer functions) and mapping to identify areas within the single field scale that are highly prone to the development of macropore flow and, thereby, have high risk of enhanced leaching of pesticides and other chemicals that are hazardous for groundwater and subsequent surface water recipients. In order to create such a pedo-transfer function (PTF) based zonation map for preferential flow risk, the following approaches were used:

1.2.1 Field scale soil texture analyses

According to the literature, soil texture is the fundamental parameter strongly influencing the physical structure of soil, hereby playing an important role in the macropore creation and water flow paths in the soils.

1.2.2 Air transport and parameters

Air transport evaluation in this study is based on the measurement of air permeability at two different soil-water matric potentials: 1) the matric potential of original samples (hereafter referred as "*ka in situ"*) and 2) the matric potential at -20 cm (*ka(-20)*). At a matric potential of -20 cm, almost all macropores of diameter ranging from 0.3 to 0.5 mm are emptied thus promoting the convective air transport

1.2.3 Water transport and parameters

The water transport in soils is characterized mainly by two types of flow soil– macropore flow and soil-matrix flow. Structured soils contain large pathways, facilitating the water transport. The two measured characteristics are *Ks* - saturated hydraulic conductivity and *k(-10)* - unsaturated hydraulic conductivity at matric potential of -10cm.

1.2.4 Leaching experiment on undisturbed soil columns

Leaching experiment has been carried out on undisturbed soil columns using Tritium as conservative tracer. 5% of the first tracer arrival time and apparent dispersivity were employed to characterize the degree of preferential flow in soils.

2 Materials and methods

2.1 Site presentation and sampling

The Silstrup field is one of the six test sites of the PLAP program. It is located in north - western part of Jutland (Figure 4) in Denmark. The geology of this area is dominated by clay-till deposits. The extent of cultivated field area is about 1.69 ha with a slight inclination of 2° to the North. Supplementary information about the site and the installed lysimetric measurement stations can be found on the web site: http://pesticidvarsling.dk/om_os_uk/uk-forside.html.

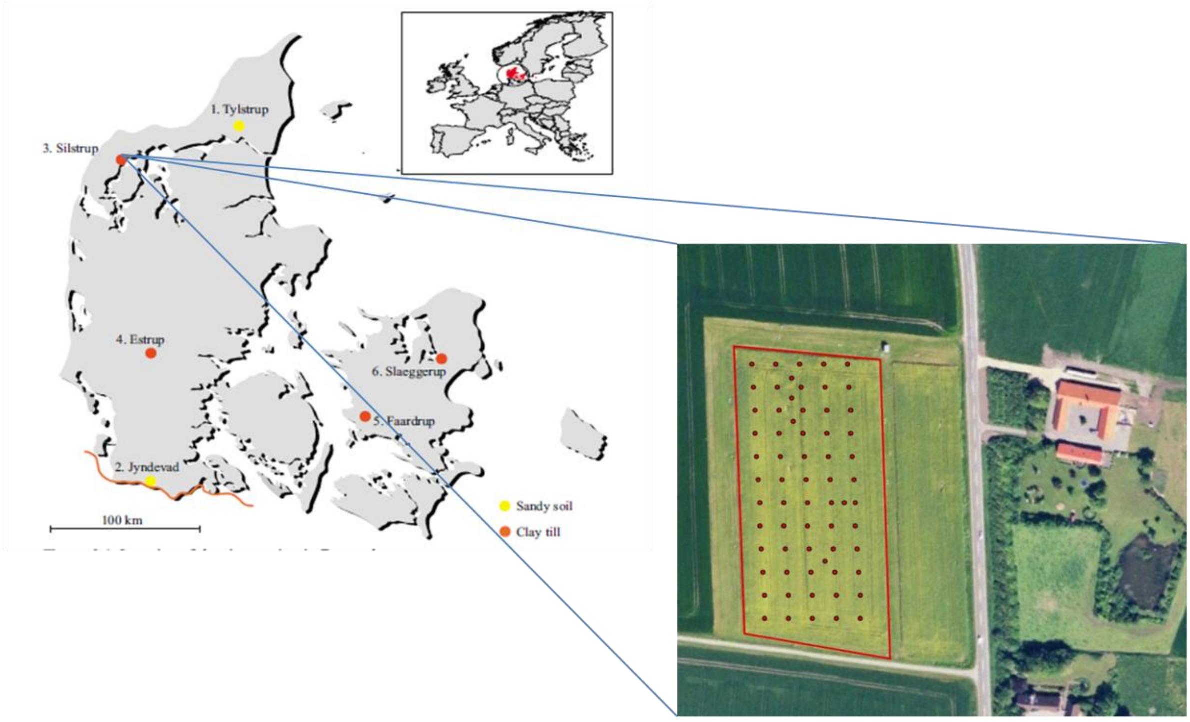

Figure 4 : location of Silstrup field

2.1.1 Sampling

65 undisturbed cylindrical soil columns (19 high x 20 cm diameter) were sampled from a rectangular grid of 15x15 m. The columns were sampled as close to the predetermined GPS sampling points as possible trying to avoid tractor tracks. The perennial grass or grass-seed production were cut off prior to the sampling. The columns were pressed into the soil as gently as possible using a hydraulic press mounted on a tractor. In order to protect the steel cylinder and to avoid compaction of the soil, a steel flange was placed on the top of the cylinder before pressing it into the soil. After pressing the cylinder into the soil, the core was excavated, the columns were trimmed carefully using a knife, and closed with plastic lids. The samples were stored at 2-5^{o}C in order to suppress biological activity. We also took 65 bulk soil samples close to each GPS sampling point, from the same depth as the soil columns for texture analysis.

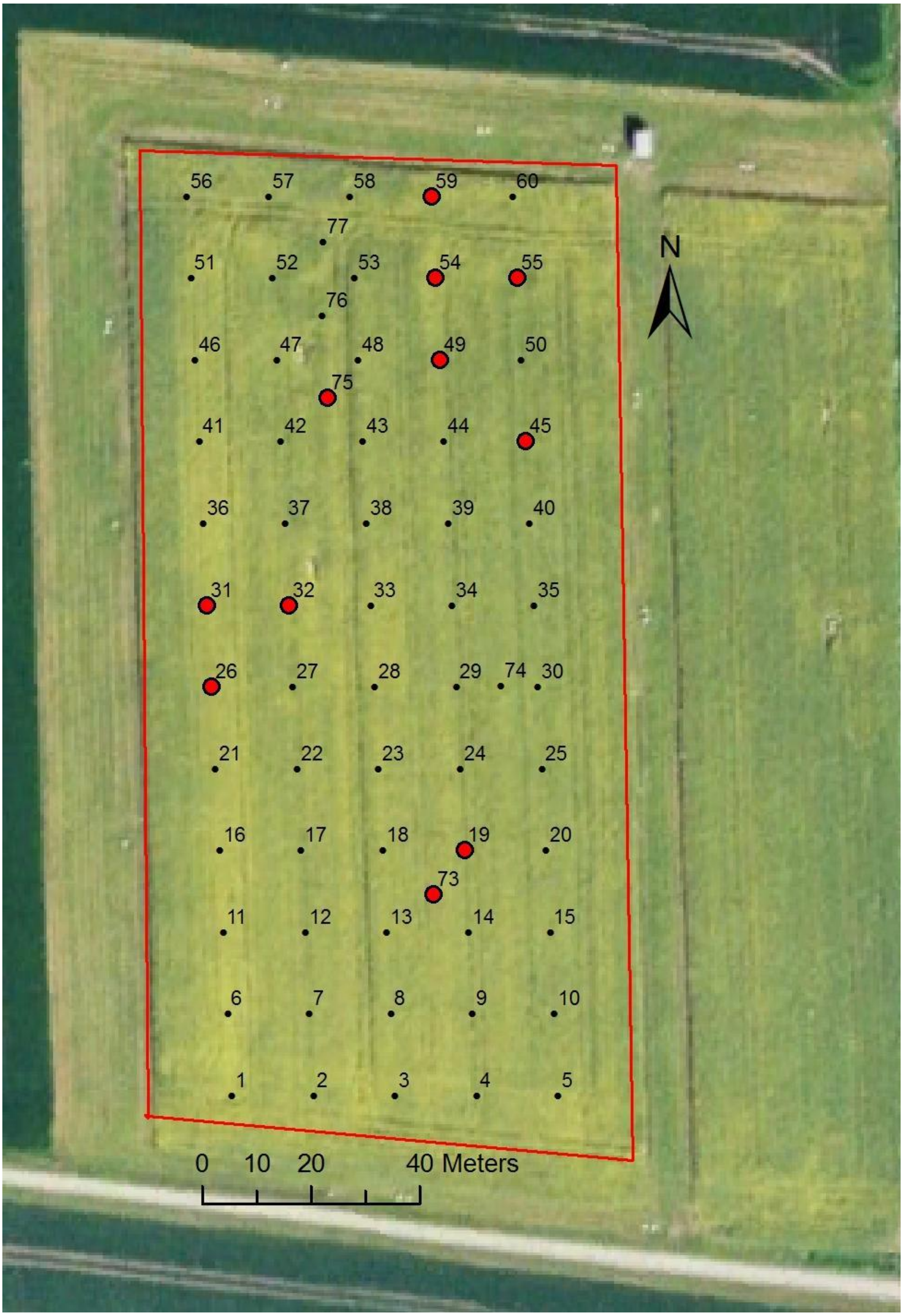

Figure 5 map showing the grid of sampling points (in black) and measurement points of hydraulic conductivity (in red)

The whole process of undisturbed samples treatment and analyses in laboratory is resumed in Figure 6:

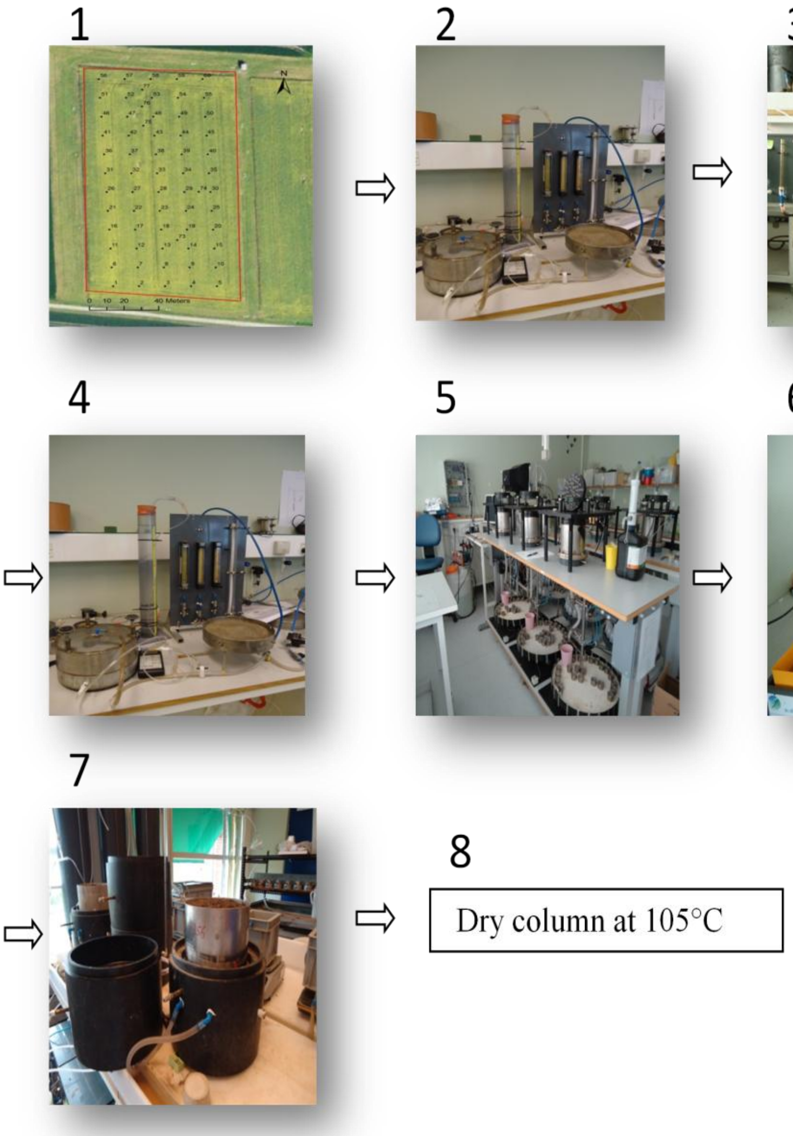

Figure 6. Different treatments and analyses on undisturbed soil columns 1) sampling ; 2) k in situ air permeability, 3) saturation and drainage, 4) ka[-20cm], air permeability at -20 cm 5) leaching experiment, 6) unsaturated hydraulic conductivity k[h]; saturated hydraulic conductivity Ks, dry column at 150°C to calculate bulk density

2.2 Texture analysis

Soil texture is a characteristic used to describe the grains and mineral particle sizes in soil sample. According to the U.S Department of Agriculture classification, the three main categories of soil textures are clay, silt and sand. The smallest particles with a diameter smaller than 0.002 mm are of clay size; silt has a range from 0.002 mm - 0.05mm, and sand a range from 0.05 mm - 2mm. Particles larger than 2 mm (gravel) are usually not considered to play a major part in the soil processes.

2.2.1 Standard particle-size measurement

The texture analysis was carried out on the bulk soil samples. Before the particle analysis, the soils were air-dried and passed through a 2-mm sieve. Standard particle size determination was performed using hydrometer and sieve analysis, based on method described by Gee and Or (2002).

2.2.2 Total organic carbon analysis

Total organic carbon of each of the 65 samples was determined by LECO 1000 CNS analyzer after combusting at 1650°C and subsequent infrared detection of CO_2 according to the method described by Tabatabai and Bremner (1970).

2.3 Air permeability measurement

Immediately after sampling, a measurement of air permeability was carried out in laboratory. Subsequesntly, the columns were saturated from the bottom by an artificial soil water solution (0.6552 mM NaCl, 0.025 mM KCl, 1.842 mM $CaCl_2$ and 0.255 mM $MgCl_2$, pH = 6.38; EC = 0.6 mΩ) during approximately 3 days and drained to a matric potential of -20 cm relative to the top of the column, during 3 days as well. After saturation and drainage, the columns were weighed and air permeability was measured again. The air permeability measurement is based on the steady-state method described by Iversen et al., (2001)

2.4 Leaching experiment

The columns were placed on a steel grid with a mesh size of 1mm. A solution of artificial rain water (0.012 mM $CaCl_2$, 0.015 mM $MgCl_2$ and 0.121 mM NaCl, EC=22.5-27 mΩ, Ph= 5.76-7.26) was supplied with an intensity of 10-mm/hour to the soil surface using a rainfall simulator consisting of 44 hypodermic needles to ensure a homogenous application. The outflow was collected through a funnel leading down to 25 plastic bottles rotating automatically. The sampling interval was 10-min for 9 first bottles, 15 min for next 12 bottles, and 30min for the last 4 bottles. The breakthrough time was registered for the first drop of exiting the column. When the outflow became steady, tritium was applied as a pulse during 10 minutes, with the same irrigation intensity as the rain fall simulator. The effluent solution collected in the bottles was analysed for turbidity, pH and electrical conductivity, and tritium. The tritium activity was determined using liquid scintillation counting (Parkard 2250 CA, Downers Grove, IL) by mixing 1ml of solution with 2ml of distilled water and 17ml of Ultima Gold scintillation cocktail (Parkard 2250 CA, Downers Grove, IL). The activity of tritium in the input solution was determined likewise, and hence a relative concentration could be determined.

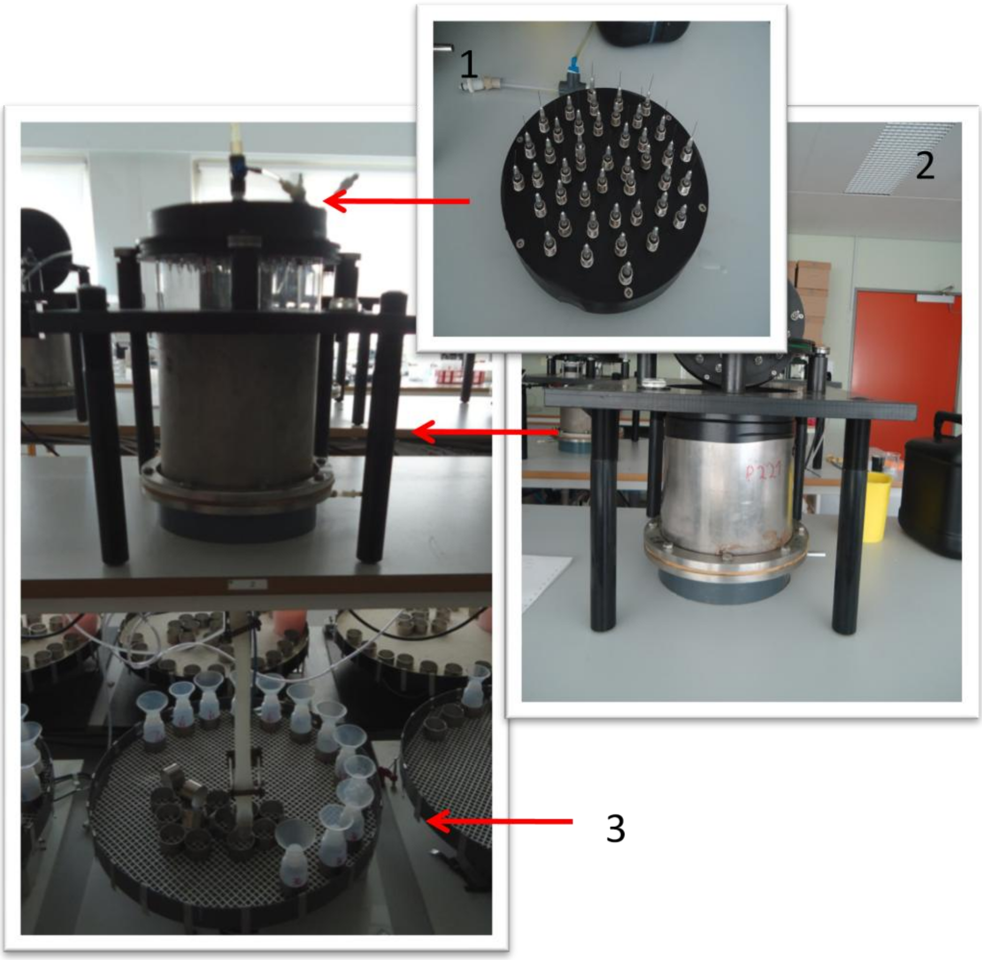

Figure 7 Setup of leaching experiment 1) rainfall simulation, 2) soil columns 3) carousel with the sampling bottles and the funnel

2.5 Hydraulic conductivity measurements

2.5.1 Unsaturated hydraulic conductivity

The soil samples were placed on a ceramic plate to measure soil hydraulic conductivity using a drip infiltrometer (van den Elsen et al., 1999). The drip infiltrometer measures the unsaturated hydraulic conductivity (*k(h)*) in the wet (near saturation) range at matric potentials (*h*) between approximately –2 to –100 cm. Five tensiometers were placed in the soil column and a water flux was applied with a needle device to the top of the sample. The measurements started as close to saturation as possible while applying a constant suction to the bottom of the soil core. When a steady-state pressure head was reached, the flux density was determined. This, together with measurements of the pressure head gradient, yielded *k* (*h*) at the resulting values of *h*. Subsequently, the flux rate was decreased and the procedure described above repeated while measuring at a lower pressure head.

2.5.2 Saturated hydraulic conductivity

After measurement of the *k*(*h*), the soil columns were re-saturated overnight and K_s was determined using the constant head method suggested by Klute & Dirksen (1986).

2.6 Calculation

2.6.1 Leaching experiment

In this study, the transfer function (or probability density function - *pdf*) (Jury and Roth, 1991) was employed to fit the breakthrough curves using the statistical program R (The R Foundation for Statistical Computing, 2011). The two main equations used are log-normal Equation [2.1] and double-log normal Equation [2.2]. These two models are based on the stochastic-convection concept and assume no dispersion condition as a fitting parameter in the formula**.**

Log Normal: $$f_{L1} = \frac{1}{[\sqrt{2\pi}\sigma_{ln}t]} exp\left[-\frac{(\ln(t)-\mu_{ln})^2}{2\sigma_{ln}^2}\right] \quad [2.1]$$

Double log-Normal:

$$f_{L2} = w_1\left(\frac{1}{[\sqrt{2\pi}\sigma_1 t]} exp\left[-\frac{(\ln(t)-\mu_1)^2}{2\sigma_1^2}\right]\right) + w_2\left(\frac{1}{[\sqrt{2\pi}\sigma_2 t]} exp\left[-\frac{(\ln(t)-\mu_2)^2}{2\sigma_2^2}\right]\right) \quad [2.2]$$

Where $w_1 + w_2 = 1$

+Expected value of *t* E(t) [T] or the average of the travel time is given by equation :

$$E(t) = \frac{m_1}{m_O} = \mu_1 \qquad [2.3]$$

where m_O is the 0th temporal moment and m_1 is the 1st temporal moment :

$$m_O = \int_0^{\infty} f dt \quad ; m_1 = \int_0^{\infty} t f dt$$

+Apparent dispersivity λ_{app} [L] is given by :

$$\lambda_{app} = \frac{\mu_2 L}{2\mu_1^2} = \frac{CV^2 L}{2} \qquad [2.4]$$

where μ_2 is the second temporal moment or Variance σ of the *pdf*. CV [-] stands for coefficient of variation, L is length of column [L]. In this study, L equals 20cm:

$$\mu_2 = \frac{1}{m_o}\int_0^{\infty} (t - \mu_1)^2 f dt \ ; \qquad \text{CV} = \qquad \frac{\sigma}{E(t)}$$

+ 5% of the first tracer arrival times is calculated by :

$$t_{0.05} = \ \mu_1 p_{0.05}$$

where $p_{0.05}$denotes for 5% quantile from transfer function.

2.6.2 Fitting of hydraulic conductivity

The measured data of hydraulic conductivity *Ks* and *k[h]* were fitted to the Van Genuchten model (1980) including the statistical pore-size distribution model of Mualem (1976) and combined with the scaling function P_m of (Børgesen et al. 2006).

$$K(S_e) = k_0 S_e^l \left[1 - \left(1 - S_e^{l/m}\right)^m\right]^2 P_m \qquad [2.5]$$

Where k_0 is the unsaturated hydraulic conductivity at h_m, *K(Se)* is the saturated hydraulic conductivity [L.T^{-1}], *l* is an empirical pore-connectivity parameter estimated to be about 0.5 as an average for many soils (Mualem 1976), and S_e is the effective saturation (van Genuchten, 1980) given by:

$$S_e = \frac{\theta - \theta_r}{\theta_s - \theta_r} = \begin{cases} \frac{1}{[1+|\alpha h|^n]^m} \ , & h<0 \\ 1 \ , & h \geq 0 \end{cases} \qquad [2.6]$$

where α [L^{-1}], n are curve shape parameters and m=1-1/n. The parameters $\theta, \theta_s, \theta_r$ are denoted actual, saturated (s) and residual (r) water contents [$L^3.L^{-3}$] respectively.

The empirical scaling function P_m equation gives a more realistic curve shape to the conductivity function in the near saturated region of the hydraulic conductivity curve.

$$P_m = \begin{cases} \left(\frac{1}{|h|\chi+1}\right)^f, & h \geq h_m \\ \left(\frac{1}{|h|\chi+1}\right)^f, & h \leq h_m \end{cases} \qquad [2.7]$$

where h_m is a parameter that can be interpreted as the boundary between pressure heads at which macropore flow or matrix flow dominates and χ=1hPa^{-1} is constant to make the scaling factor dimensionless. Without prior knowledge of pore size boundary between the two domains, the h_m parameter is a fitting parameter and the f-parameter is a shape parameter of the conductivity function.

2.6.3 Prediction of hydraulic conductivity

Soils saturated hydraulic conductivity (*Ks)* is an important soil physical property and essential input to the most simulation models used in soil and land research (Nemes et al., 2005). Both laboratory and field measurement are usually time consuming, expensive and labor intensive. Pedo-transfer function was introduced by Bouma over the 1980s to estimate soil hydraulic properties by using the most common parameters (texture and bulk density). There have been many PTFs introduced for different types of soil and climates. In this study, the prediction of both *Ks* and *k[h]* used neural network model to develop PTFs. An advantage of neural networks compared to more traditional regression PTFs is that they require no a priori assumption. This model was developed by Iversen and Børgesen (2011), using Neural Network Toolbox in MATLAB (Demuth and Beal, 2000) with the same 6 hidden nodes (Schaap and Bouten 1996) for the 7 classes of texture, humus, OC, bulk density used as predictors (see Iversen et al., 2011 for more details). Other PTFs model has been used to predict *Ks* such as Vereecken et al. (1990) using a dataset for the Belgium soils:

$$\text{Ks (cm day}^{-1}) = e^{[20.62-0.96(\ln C) - 0.66(\ln S) - 0.46(\ln OM) - 8.43(Db)]}$$

where C is clay, S is sand, OM is organic matter, Db is bulk density

3 Results

3.1 Texture analyse

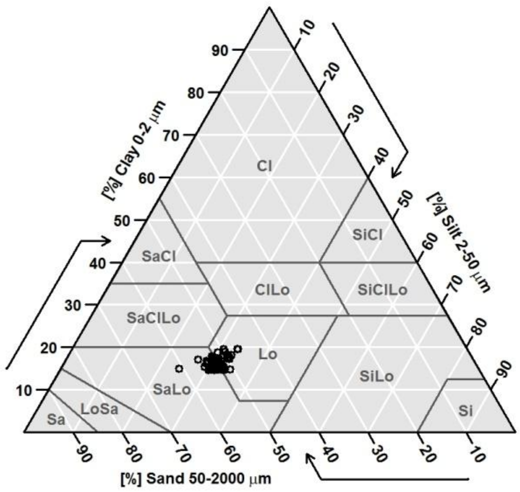

Figure 8 : Triangle of soil texture of 65 columns from Silstrup field

Figure 8 shows the soil types from the Silstrup field which are mainly of loamy or loamy-sandy texture. This texture represents a common soil in Denmark. Details of the soil texture results within 7 textural categories can be found in Appendix 1.

The contour map of the soil clay content resulting from the texture analysis (Figure 9a) of the samples from a rectangular grid of 15x15m was interpolated using ArcGIS 10 (ESRI). It shows a contrast of clay content between the northern and southern part of the field, with higher clay contents in the northern part and the lower clay contents in the southern part of the field. Contour maps of the sand and silt fractions can be found in Appendix 2

Total organic carbon (TOC) from texture analyses varied from 1.7% to 2.2% with the average value of 1.96%. The contour map of TOC is shown in Figure 9b.

The dry bulk density (ρ_b) [g cm^{-3}] is determined by dividing the dry solid mass by the total volume of soil:

$$\rho_b = \frac{m_s}{v}$$

The bulk densities of the soils samples from the Silstrup field ranged from 1.39 to 1.6 g.cm^{-3} with an average value of 1.49 g.cm^{-3}. The highest bulk densities are found in the upper third part of the field (Figure 10).

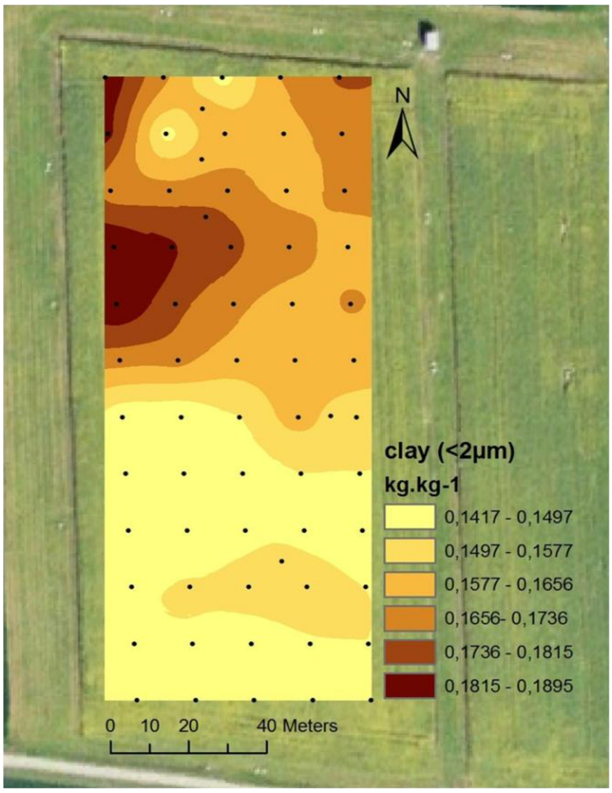

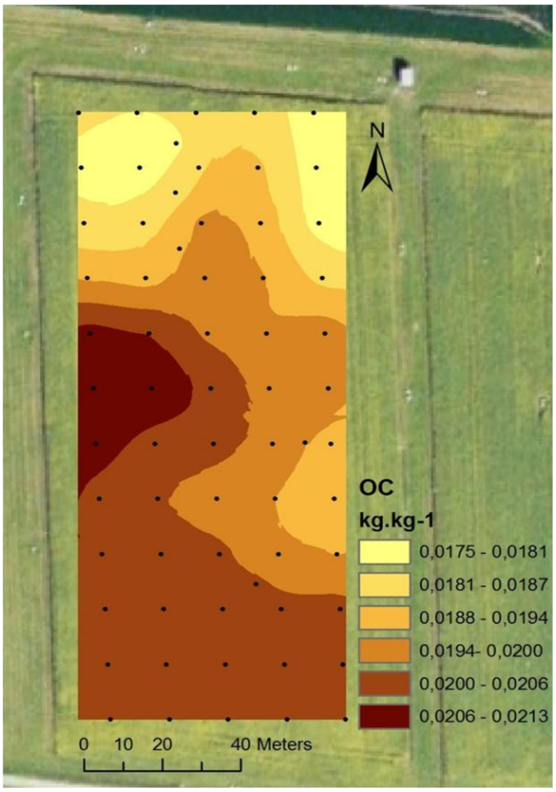

Figure 9 : Contour map of a) the clay content b) the TOC

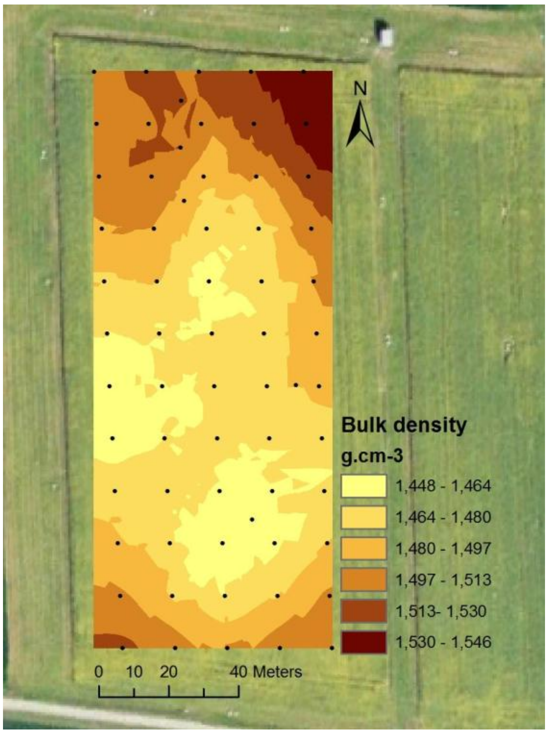

Figure 10 : Contour map of bulk density

3.2 Air transport

Air permeability (k_a) is a pressure-driven gas transport parameter and is governed by pore size distribution, air-filled pore space and the continuity of large-pore networks (Buckingham, 1904, Osozawa, 1998, Moldrup et al., 1998, Kawamoto et al., 2006)

At wetting condition, the soil moisture is elevated; soil pores are filled with water and the air transport is very small compared to the dry conditions. The contour maps of air permeability *in situ* and at matric potential of -20cm are shown in Figure 11. The contour map of air permeability at matric potential of –20cm was created without six missing values from the first six columns (corresponding to the points number 1-6, Figure 5) from the southern part of the Silstrup field.

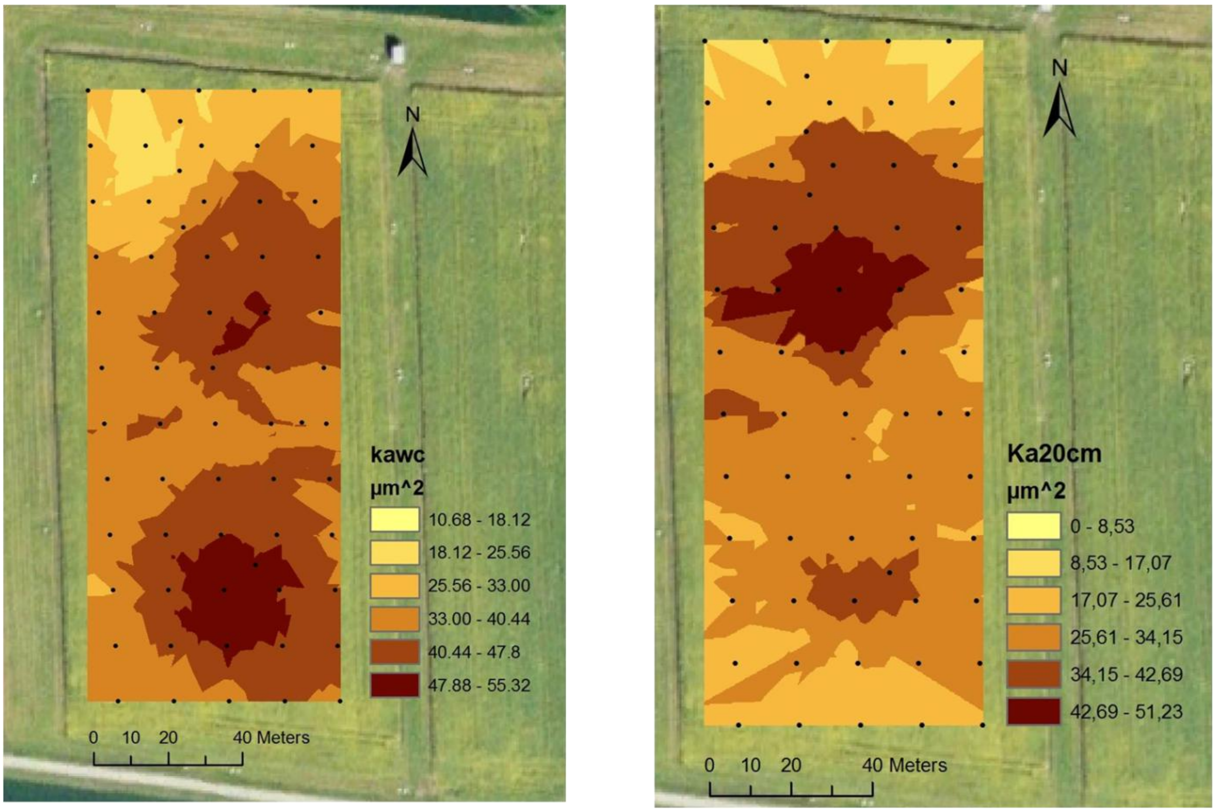

Figure 11: Contour map of a) air permeability in situ, b) air permeability at matric potential of -20cm

3.3 Water transport

3.3.1 Data analyses

The measurement of saturated and unsaturated hydraulic conductivity was carried out on 11 columns from the Silstrup field (the location of these 11 columns can be found in Figure 5 - red points) and additional 15 columns from the Faardrup field, which is another test site of PLAP. The soil also consists of clay till but has a different range of clay content. The published data from Iversen et al., (2011) with the high range of clay content were collected and analyzed as well.

In Figure 12, log(*Ks*) is plotted as a function of the OC, clay content, bulk density and both values of air permeability. Among the three parameters of texture analyses, the highest correlation related to the bulk density with R^2=0.50, log(*Ks*) showed a slightly negative correlation with OC and clay content. log(*Ks*) is positively correlated with both types of air permeability measurements.

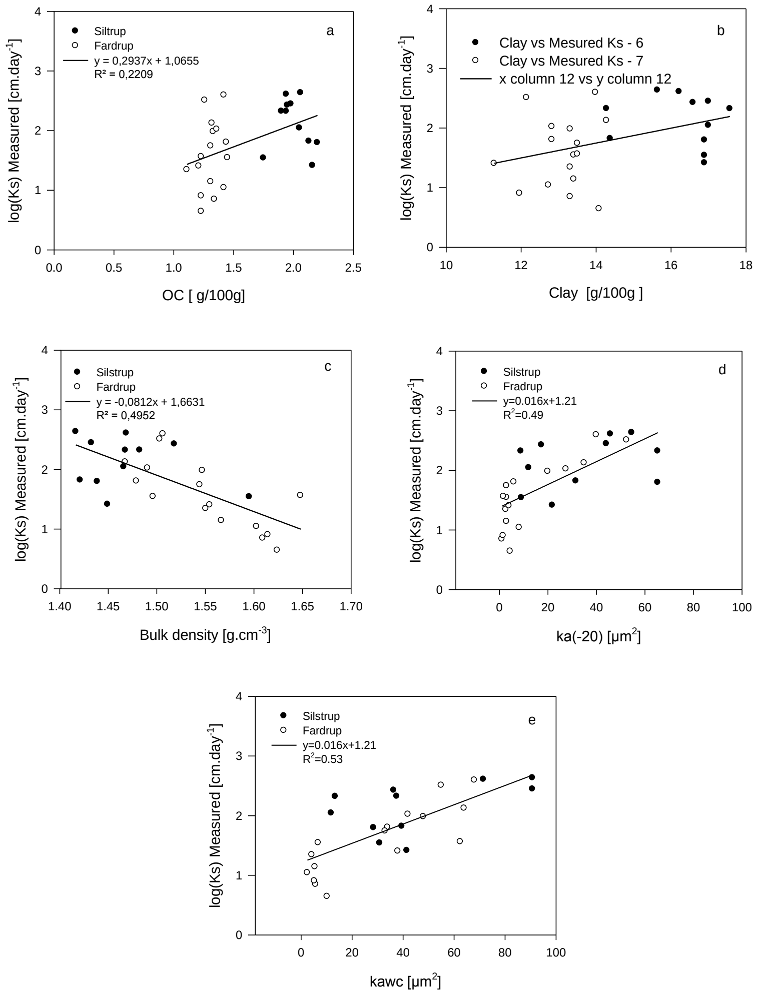

Figure 12 : The plot of log(*Ks*) as a function of a) OC, b) Clay, c) Bulk density, d) ka(-20) e) ka in situ

Figure 13 shows the correlation of log(*k(-10)*) with the soil texture analyses and air transport parameters. The highest correlation of log(*k(-10)*) is found with clay content with R^2= 0.36, and OC with R^2=0.22 . There is no correlation with bulk density and air transport parameters.

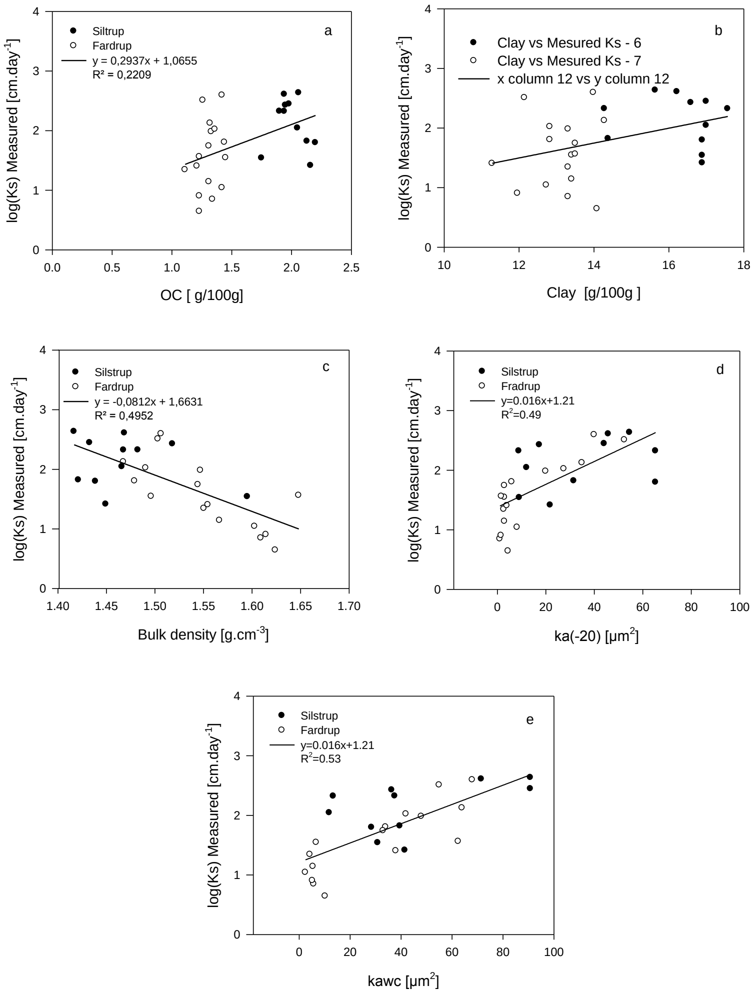

Figure 13 : The correlation of log(k[-10]) with a) OC b) clay content c) bulk density d) ka(-20) e) ka in situ

3.3.2 Prediction of hydraulic conductivity

The prediction of unsaturated hydraulic conductivity at log (*k[-10]*) using a neuron network model gives better results than prediction of saturated conductivity log(*Ks*) showing the RMSE of 0.31 and 1.17 respectively (figure 14).

Computed values of log (*Ks*) derived from Vereecken´s model (Figure 14a) are underestimated compared to the measured values, with an average of log (*Ks*) = 1.04 cm.day^{-1}.

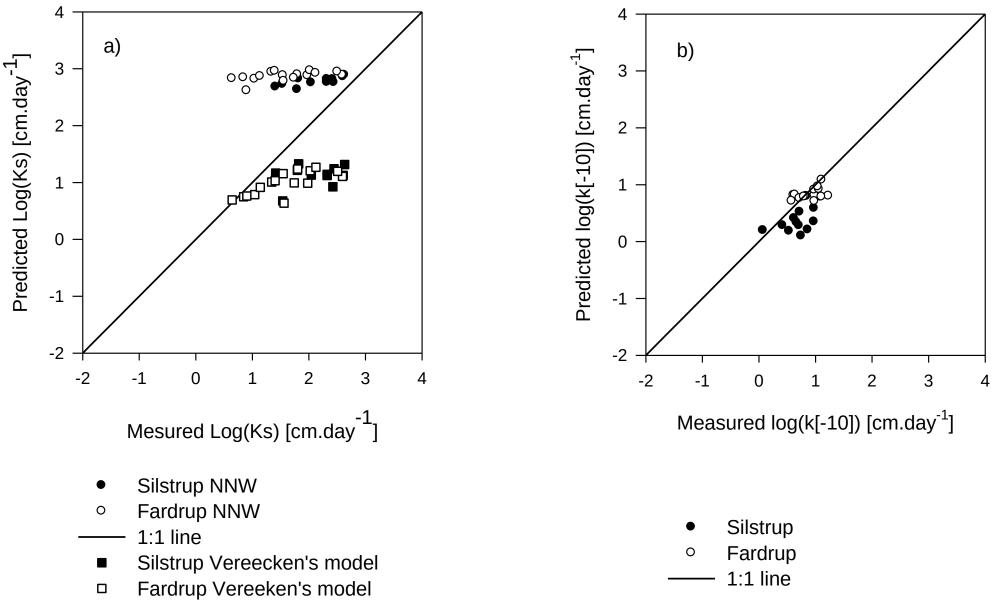

Figure 14 : Measured values plotted against estimated values at a) log(Ks) b) log(k[-10]).

3.4 Leaching experiment

3.4.1 Tritium recovery and 5% tracer arrival times

The relative arrival time of first 5% of the tritium tracer mass was interpolated from mass accumulated tritium curves. According to Knudby and Carrera (2005), this parameter could be considered as the best indicator of preferential flow and transport. The contour map of 5% arrival times is shown in the Figure15a.

The tritium recovery was in average of 65% for all columns. Among 65 columns, only one column reached closely to 100% of tritium recovery, 10 columns had a tritium recovery higher than 80% and 29 columns around 70%. The average sampling time was 5.5 hours. The contour map of tritium recovery is shown in Figure 15b.

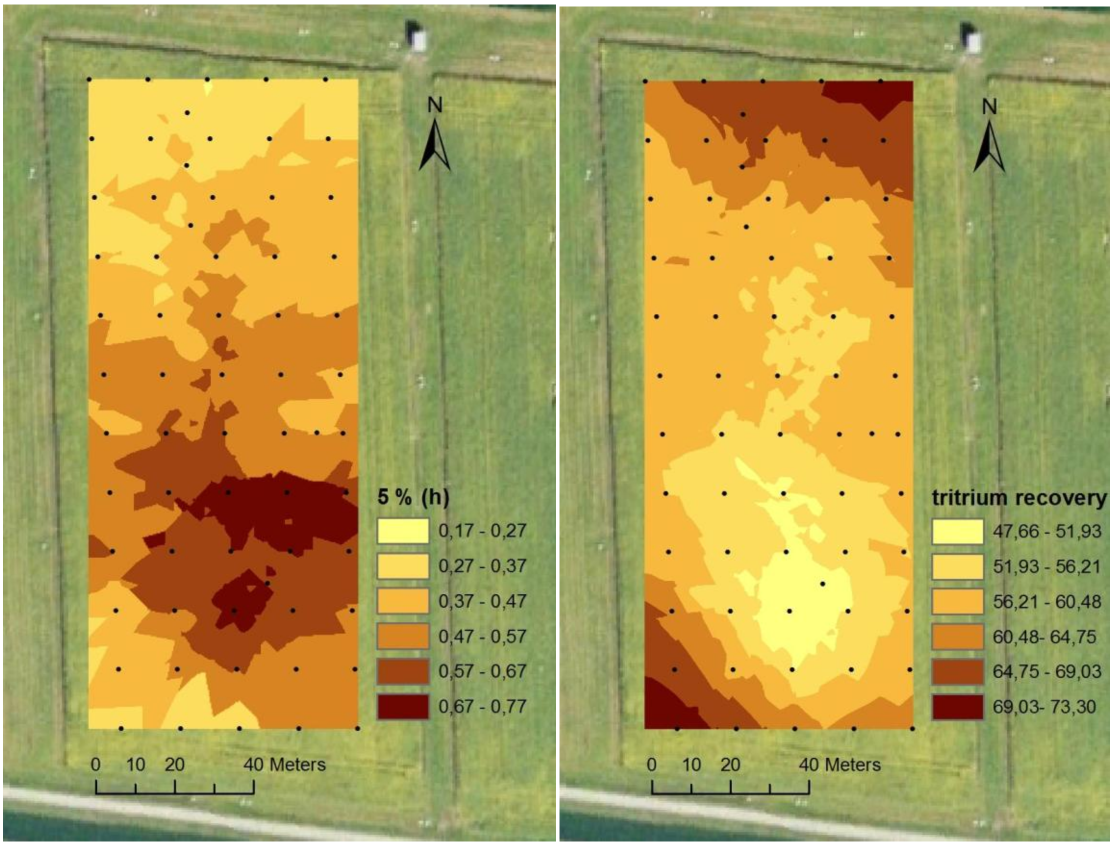

Figure 15: Contour map of a) 5 % of arrival times, b) tritium recovery

The correlation of 5% arrival times with other soil parameters are summarized in Table 1. and v

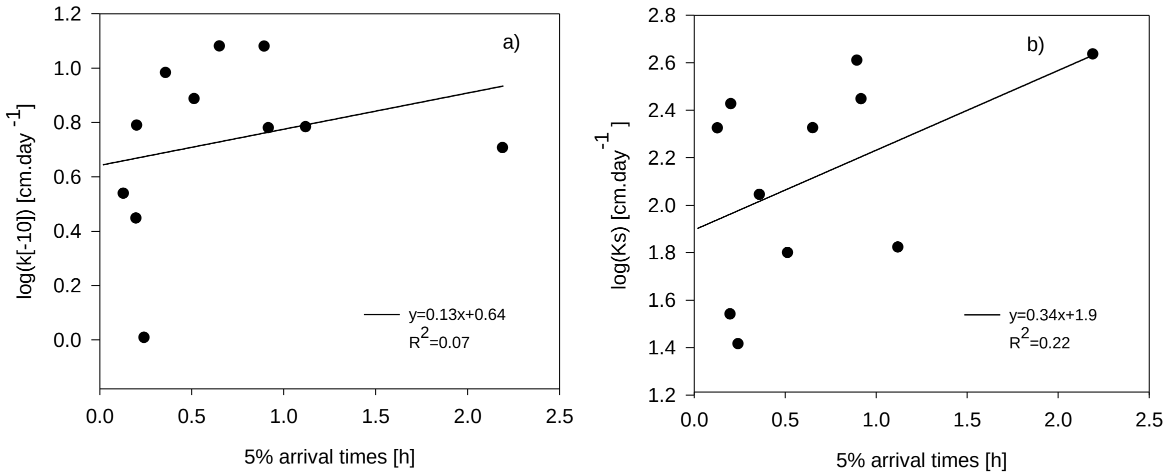

isualized on figures 16 and 17.

Figure 16 : The plot of 5% arrival times versus a) log([k[-10]) b) log(Ks)

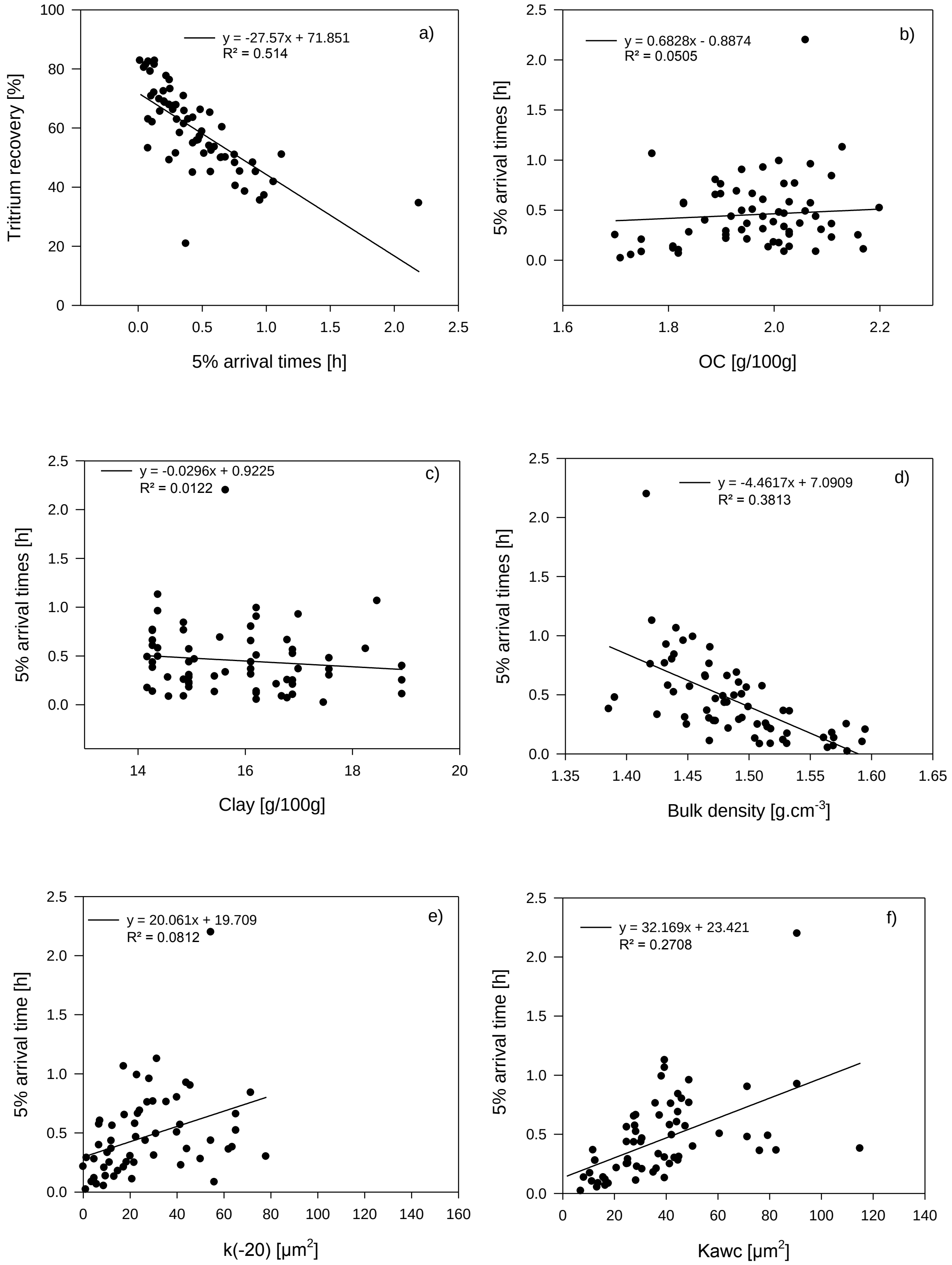

Figure 17 : The plot of 5% arrival times as a function of a) tritium recovery b) OC c) clay content d) bulk density e) air permeability at matric potential of -20cm, f) air permeability in situ.

Table 1 Results of Pearson's correlation matrix

		OC	Clay	Bulk density	ka (in situ)	Ka(-20)	Log(Ks)	Log(k[-10])	5% arrival times	^{3}H recovery
OC [g.100g^{-1}]	Pearson Correlation	1								
	N	81								
Clay[g.100g^{-1}]	Pearson Correlation	,552**	1							
	N	81	81							
Bulk density [g.cm^{-3}]	Pearson Correlation	-,557**	-,217	1						
	N	81	81	81						
Ka(insitu) [µm^2]	Pearson Correlation	,211	,082	-,523**	1					
	N	81	81	81	81					
Ka(-20) [µm^2]	Pearson Correlation	,404**	,084	-,524**	,602**	1				
	N	74	74	74	74	74				
Log(Ks) [cm.day^{-1}]	Pearson Correlation	,463*	,399*	-,658**	,734**	,699**	1			
	N	27	27	27	27	27	27			
Log(k[-10]) [cm.day^{-1}]	Pearson Correlation	-,327	-,472*	-,045	-,083	,035	,139	1		
	N	27	27	27	27	27	27	27		
5% arrival times [h]	Pearson Correlation	,225	-,111	-,618**	,520**	,360**	,477	,257	1	
	N	64	64	64	64	58	11	11	64	
^{3}H recovery [%]	Pearson Correlation	-,164	,074	,753**	-,589**	-,453**	-,423	-,468	-,717**	1
	N	65	65	65	65	58	11	11	64	65

**. Correlation is significant at the 0.01 level (2-tailed).

*. Correlation is significant at the 0.05 level (2-tailed).

3.4.2 Modeling and predicting of breakthrough curves

Since Equations [2.4] and [2.5] cannot be computed with time set as infinite, the numerical analyses of breakthrough curve was performed assuming almost complete (very close to 100%) tritium recovery in effluent after 3 water-filled pore-volumes.

The modeling of breakthrough curves was carried out with Equations [2.4] and [2.5]. It was found that the double-log normal model performed better than the log-normal model (Figure 18). This can be explained by the fact that since the double-log normal has more parameters, the modeled curve is fitting more accurately the measured data. However, the model did not perform so well for several columns having a very high and early peak of relative concentration (Figure 18b), leading to an underestimation of the certain parameters computed by the model.

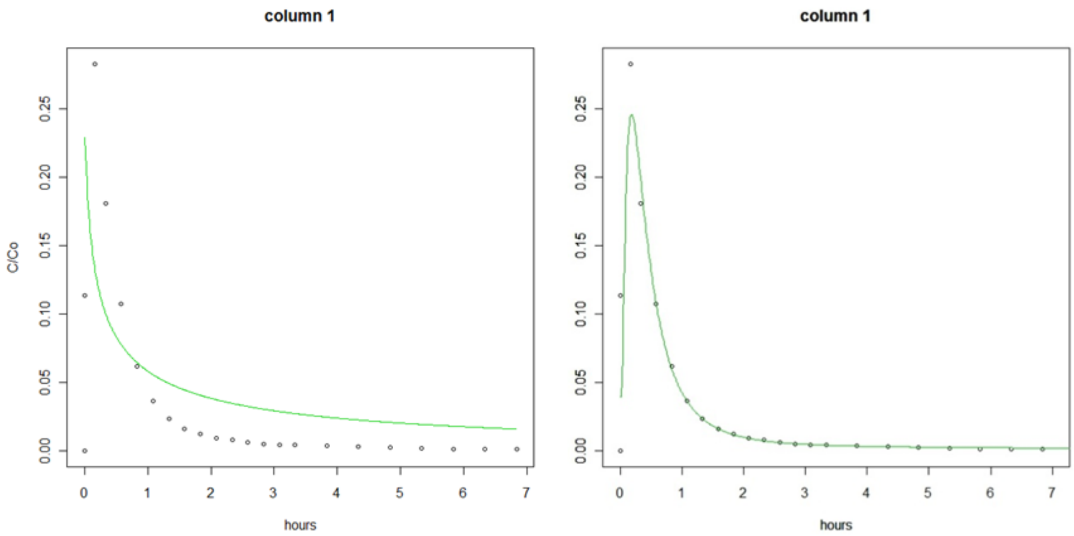

Figure 18 : The fit of modeled curve to the measured data, on the left using log normal, on the right using double lognormal equation.

The shapes of breakthrough curves are very variables (Appendix 3), showing that the field is very heterogeneous. A few of them have a high peak, positive skewness, and very long tailing (for example column 1, figure 18, right), suggesting a high degree of macropore flow. Most of them show a medium peak, positive skewness and long tailings (Figure 19a). The rest of soil columns have an unclear peak due to the dominating of matrix flow in the column (Figure 19b).

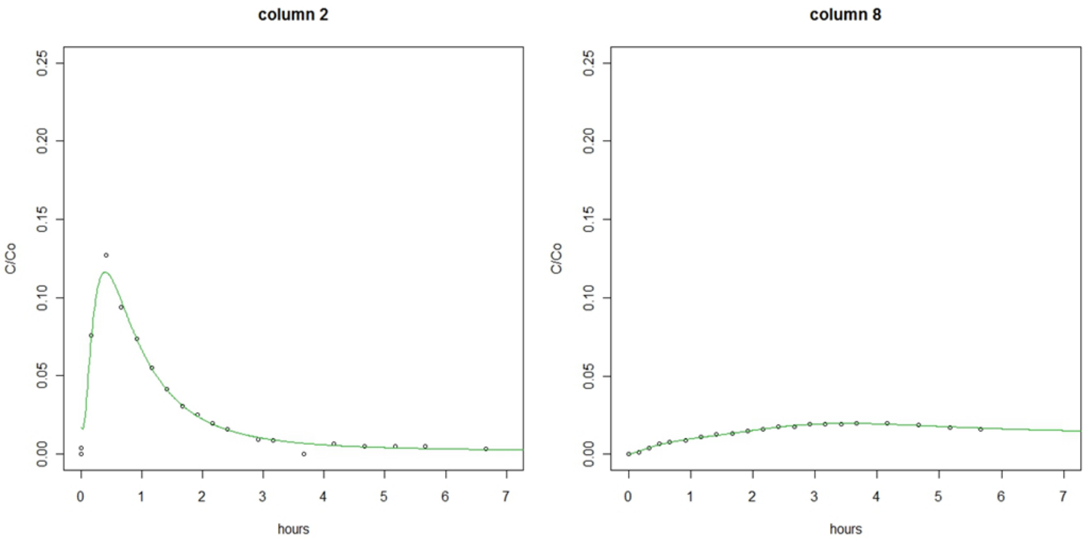

Figure 19 : On the left, column 2 showing a BTC with a medium-high, well defined peak compared to, on the right, an unclear location of peak for column 8, on the right

The apparent dispersivity was calculated using Equation [2.4] and the result is shown in Figure 20

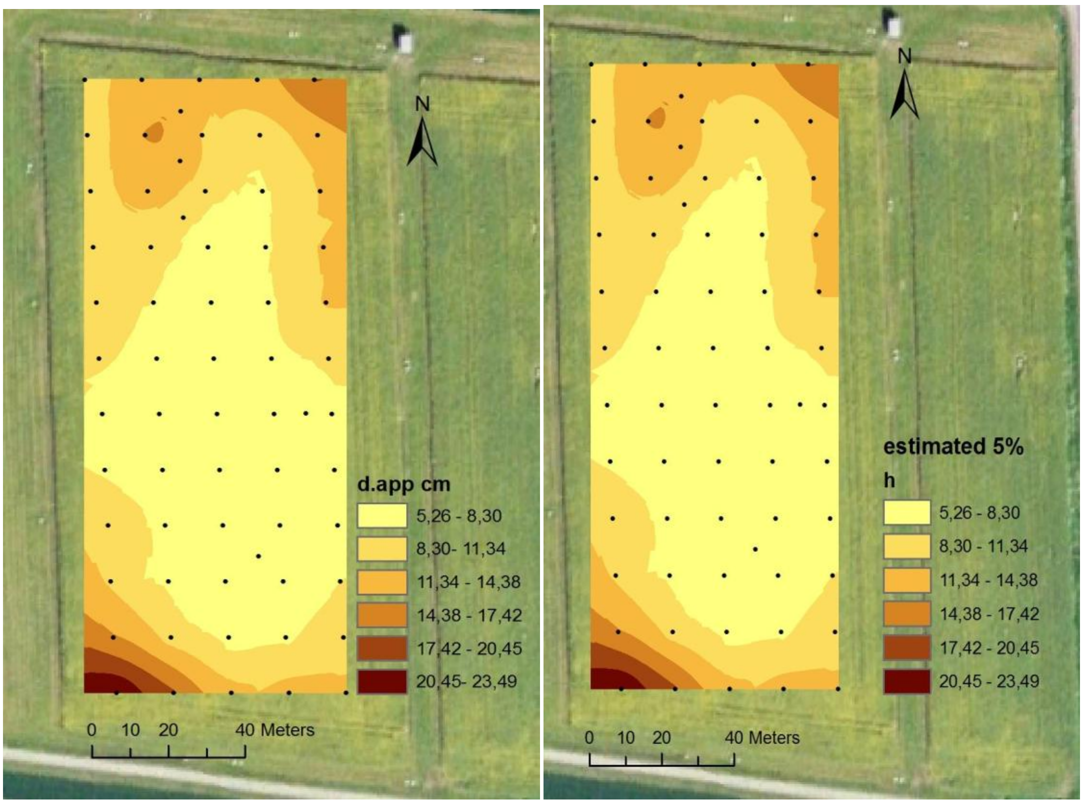

Figure 20 : contours map of apparent dispersivity on the left and 5% estimated arrival times from predictive model on the right

4 Discussion

4.1 Texture analyse

4.1.1 Soil mapping of clay content and Total Organic Carbon

Since at the beginning of the PLAP program destructive mapping methods were not allowed in the test fields. It was decided to use the non-invasive geophysical tools – like electromagnetic profiling using EM-38 sensor (Geonics Ltd., Canada) to determinate clay content in the field. The ground conductivity map was created in 1999 (Figure 21b) showing a range of apparent resistivities from 40 to 80 Ωm, with the majority of the area being within 50 to 60 Ωm. In the northern part of the field, there are two areas with apparent resistivity within the range 40 to 50 Ωm indicating higher clay content.

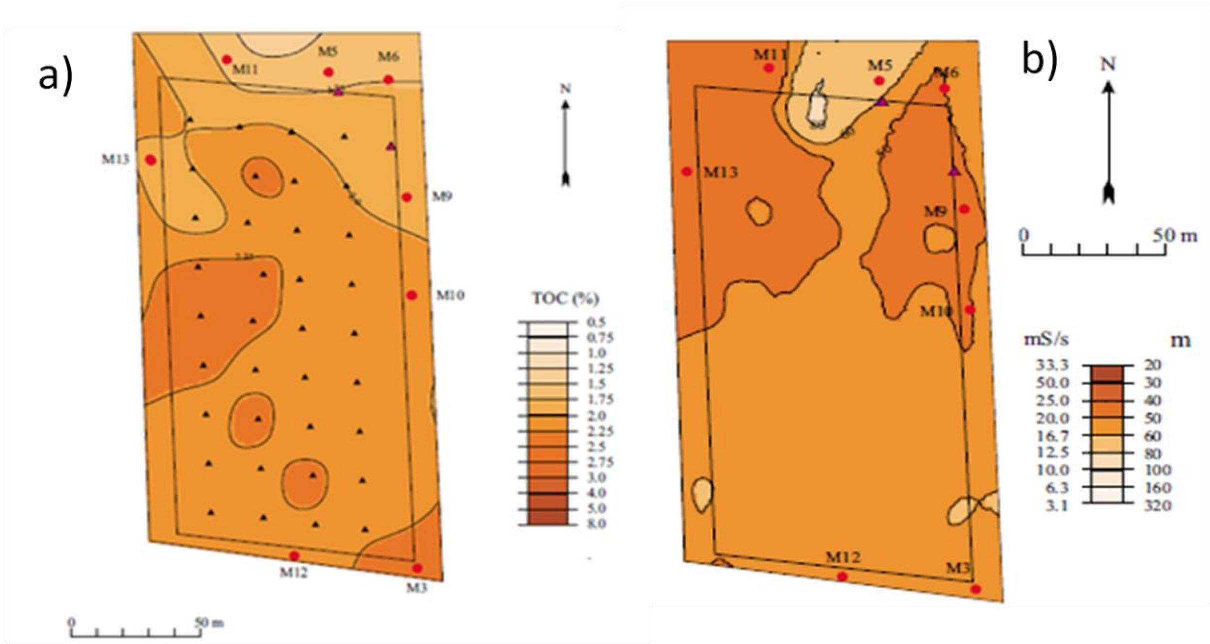

Figure 21 : a) map showing the distribution of TOC, b) map showing the distribution of apparent resistivity values, situation in 1999 (Lindhardt et al., 2001).

When comparing our results (Figure 9b) with these maps we observe that even if the ground conductivity data do not show the absolute clay content values, they reveal the same pattern of clay content repartition.

According to the Total Organic Carbon (TOC) analyses from 1999, TOC varied between 1.9% and 2.4% (dry weight) with a mean of 2.2% ± 0.1%. The concentration was lowest in the northern part of the field (Figure 21a). The comparison of the TOC content from our study to the map obtained in 1999 shows no significant changes over past ten years. According to the contour maps (Figures 9), the clay content and OC have the inverse tendencies. Moreover, the negative correlation found between OC and bulk density (r =-0.56, Table 1) shows the influence of OC on soil structure, improving its resistance against compaction.

4.1.2 The Dexter Index, n

Organic carbon, the major component of soil organic matter, is extremely important in all soils processes as it controls soil physical properties (Dexter et al., 2008). Additionally, it also mitigates climate changing aspects through its sequestration in stable forms in the soils (Satori et al., 2006). Organic carbon is known for its important role in the sorption of some organic contaminants e.g PAH (de Jonge et al., 2008, Celis et al., 2006), and pesticides (Jarvis et al., 2007; de Jonge et al., 2000) in soils as it delays the travel time of these compounds to groundwater. The increase of OM content may modify the structure of soil by replacing larger cracks and clods with more aggregated material, creating more tortuous and thinner pathways for water transport (Nemes et al., 2005).

Dexter et al. (2008) introduced the concept which states that the complex organic carbon (COC) is formed by association of clay and OC in proportion: 1g of OC associates with 10g of clay). If the ratio is above the clay saturation line (1:10) (Figure 22), the soil has more free OC and it is called NCOC (Non complexed organic carbon). These soils have a high aptitude to the sorption of organic compounds and have “strong physical properties”. To understand the term “strong physical properties” we can imagine that COC plays a role of a spring - when the soil is subjected to mechanical deformation; it quickly regains its initial state. The soils could be denoted as ´´hungry” in case of clay content below the saturation line. These soils contain more free clay and form the associations of non-complexed clay (NCC), i.e., clay that is not complexed with organic carbon. Non-complexed clay is easier dispersed in water and forms water dispersible colloids which can adsorb compounds like pesticides or phosphorus and move quickly through the macropore pathways. On the other hand, because of the clay lost by water dispersion, the macropores become larger and straighter, thus contributing to the colloid-facilitated transport (de Jonge et al., 2009). According to (Jarvis et al., 2007) the areas where the clay content is higher are prone to the development of risk of macropore flow.

The contour map of the *n*-index and the relation of clay and OC of the Silstrup field according to Dexter et al. (2008) is shown on Figure 22. The range of Dexter´s *n*-index is from 6 to 11, while the higher value is found in the northern part of field and the smaller one in the southern part. Based on this we conclude that the soil in the northern part is potentially more structured, thereby favorising the occurrence of preferential flow pathways. We expect that the Dexter number could serve as an indirect indication of macropore flow.

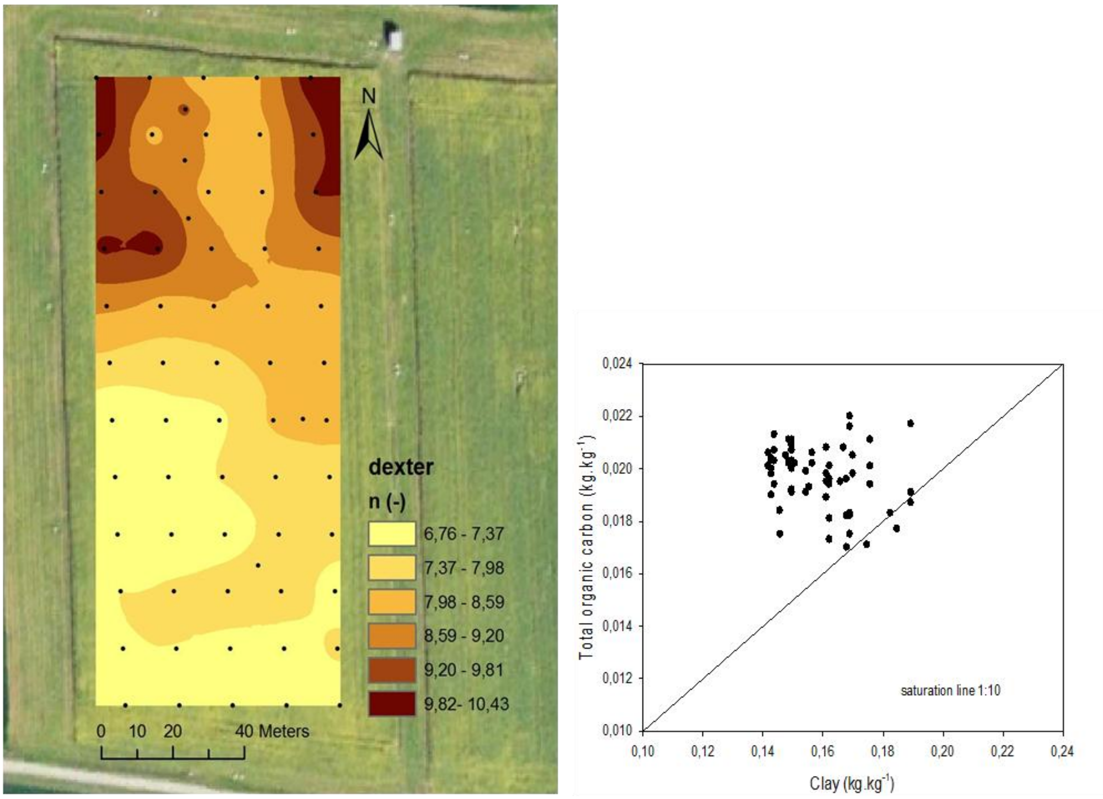

Figure 22 : On the right, a contour map showing the distribution of Dexter index. On the left, the relation between the clay content and OC of Silstrup soils.

Risk assessment of leaching pollutants in soils is not only studied at the soil surface but also to the depth of soil profile. With depth, the gradient of organic carbon decreases while clay content increases. For example, for the B-horizon of soil, the cracks often occur due to accumulation of clay and subsoil compaction by heavy agriculture machinery (Schjønning and Rasmussen; 1989). That explains the increase of hydrodynamic dispersion in this layer, as shown previously by Jury and Roth (1991) and Vanderborght et al. (2007).

4.2 Air transport parameters

The measured data of air permeability (*ka-in situ*) were plotted as a function of *ka (-20)* (Figure 23). We can observe that almost all points are situated above the line 1:1,few on them are under the line 1:1. It shows that the moisture content during the sampling was lower than at matric potential of -20cm and that the soil has been in a drier state.

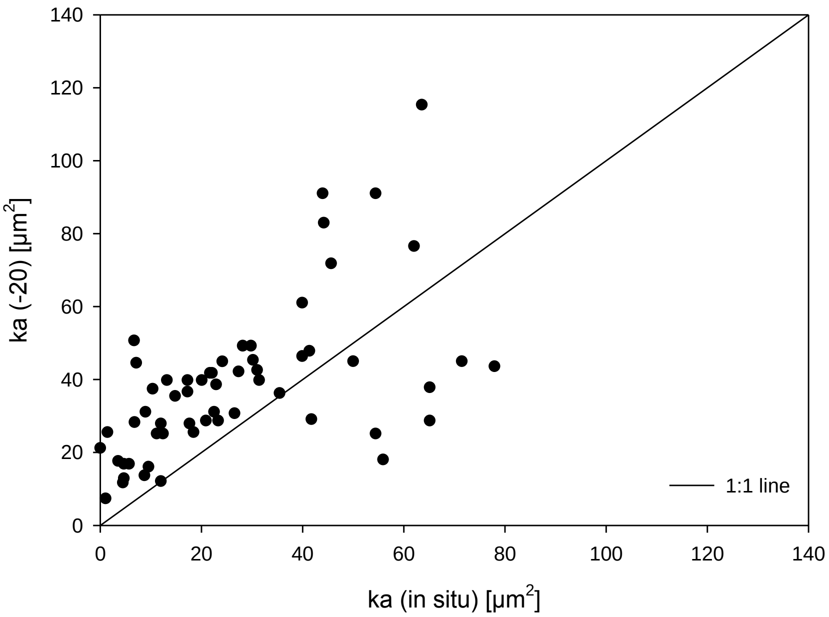

Figure 23 : The relationship between the air permeability *in situ* and at matric potential of -20 cm.

When observing Table 1, the best correlation between air transport and soil texture is found with OC, which is in an agreement with previous findings (Brandy and Weill, 2004). An increase of OC in soil will ameliorate its resistance against soil compaction. That can be proved by the negative correlations found between OC and bulk density and between OC and air permeability. According to the bibliography study (GEUS, 2009), the Silstrup field has not been ploughed since 15th of December 2008.

4.3 Water transport parameters

When the soil is characterized by a high value of bulk density, matrix-dominated water transport is reduced, while potential macropore transport may increase if there is a macropore present, since water will not flow in the compacted matrix. This explains the negative correlation found between log(Ks) and bulk density. Clay and OC show a slightly positive correlation with log(Ks). Increased OC content leads to an increase of the porosity of soils, while a higher clay content together with deformation effect of heavy machinery leads to the formation of persisting cracks in the soil profile

Water transport in soils is composed of two types of flow: macropore flow and matrix flow. If there are macropores present in soil, the macropore flow will be responsible for the majority of the water transport, according to Poiseulle's law. That explains the positive correlation found between water transport and air transport (Table 1). Under unsaturated conditions at matric potential lower than -10 cm, water transport in soil is mainly due to the matrix flow. This statement is supported by no correlation found between the log(*k[-10]*), bulk density and air permeability. The log(*k[-10]*) has negative correlation with the clay content and OC content. According to Loll et al. (1999), the air permeability can be used to predict the saturated and unsaturated hydraulic conductivity. We confirmed this statement by the high correlation found between air permeability and hydraulic conductivity, with the coefficient of determination R^2=0.53.

In order to get a better view of the prediction of log(*Ks*) and log(*k[-10]*), the hydraulic conductivity data from both fields were plotted together with the previously published data of Iversen et al., (2011) (Figure 24). One more time, we can see the results showing that log(*k[-10]*) is better predicted than log(*Ks*) with smaller RMSE = 0.57 comparing to RMSE = 0.79 for log(*k[-10]*). The soils containing more than 20% of clay reveal a high variability of hydraulic conductivities; this variability can be explained by the structure of soils dependent on presence of macropore pathways. In the sandy soils containing less than 5% of clay, the pore size is more homogenous, implying small variability of hydraulic conductivity. Therefore, the average values of log(*Ks*) are higher than for the other soil types. The risk assessment of groundwater contamination needs to consider the sandy soils because of their high values of log(*Ks*) and weak potential of pollutant attenuation due to the low OC content.

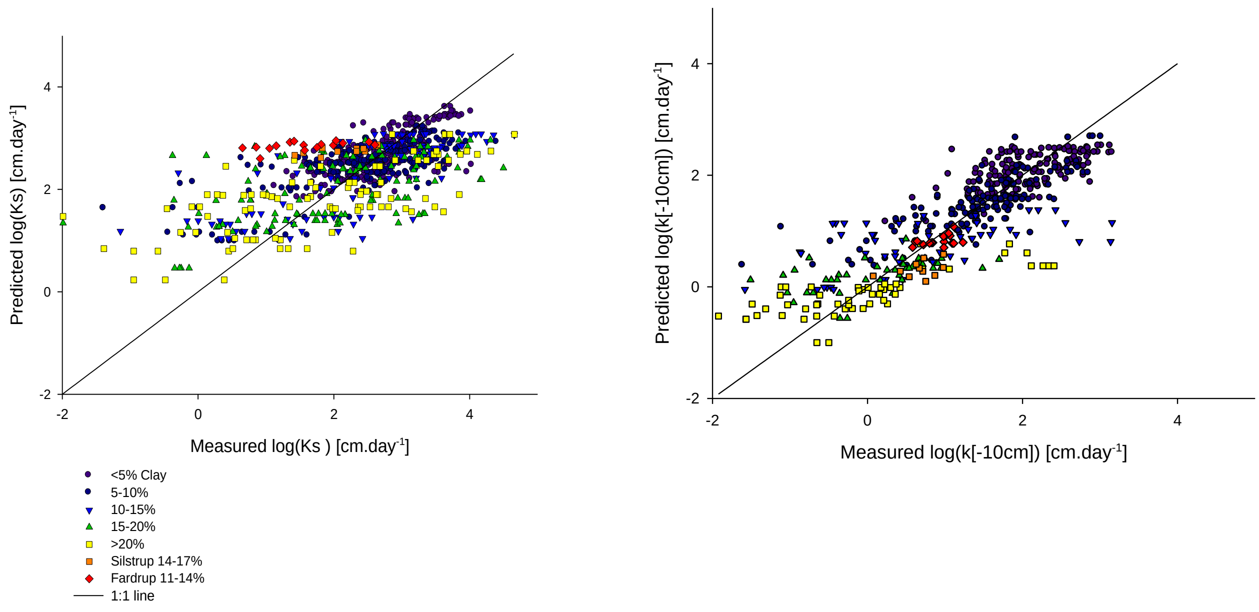

Figure 24 : The plot of measured versus predicted values of of Ks on the left and log(k[-10]) on the right . The predicted values were derived from the neuron network model.

As mentioned in introduction, the log_{jump} can be seen as an indicator of the risk of macropore flow in soils. The three dimension map of log_{jump} (Figure 25) was created using Surfer 10 (Golden Software). The high risk of macropore flow is found in the northern part of the field. Log_{jump} has a high correlation with clay content. This is not surprising since clay content was used as a predictor parameter in predictive model.

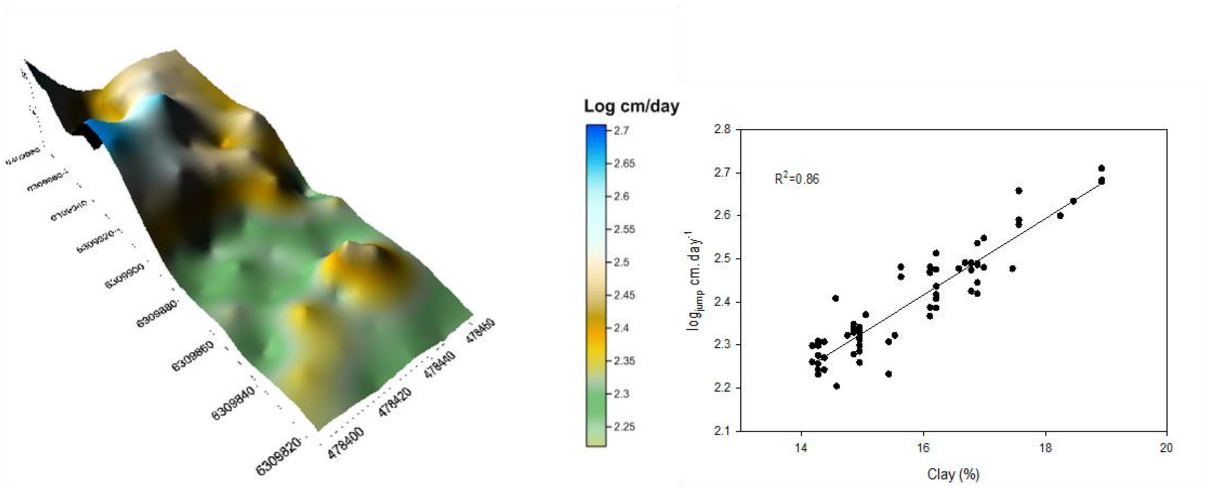

Figure 25 : a) 3D map of log_{jump} b) log_{jump} was plotted as a function of clay content

4.4 Leaching experiment

4.4.1 Tritium recovery and 5% tracer arrival times

As can be seen on the Table 1, a negative correlation was found between the 5% arrival times and tritium recovery, short 5% arrival times increasing the mass of tritium recovery in effluent and thus suggesting the fast transport of solute through the column.

It is interesting to observe that the highest correlation is found when plotting 5% arrival times against bulk density (Table 1). It confirms that compacted soil structure creates preferential transport pathways leading to short residence time of tracers. However, contrary to what we expected, the 5% arrival times do not show any correlation with clay content. This could be due to the small range of clay content, causing that the correlation is insignificant. Bulk density is not only influenced by the soil texture but also by the soils management practices. Figure 26 illustrates two blocks of soils having a different degree of compaction. The block *b* is the example of highly-compacted soil where the micropores are suppressed and the macropores become larger, promoting the water transport through persistent cracks. In the case of the block *a*, the water transport is supplied by both types of flow: matrix flow through soil matrix and macropore flow through the macropores.

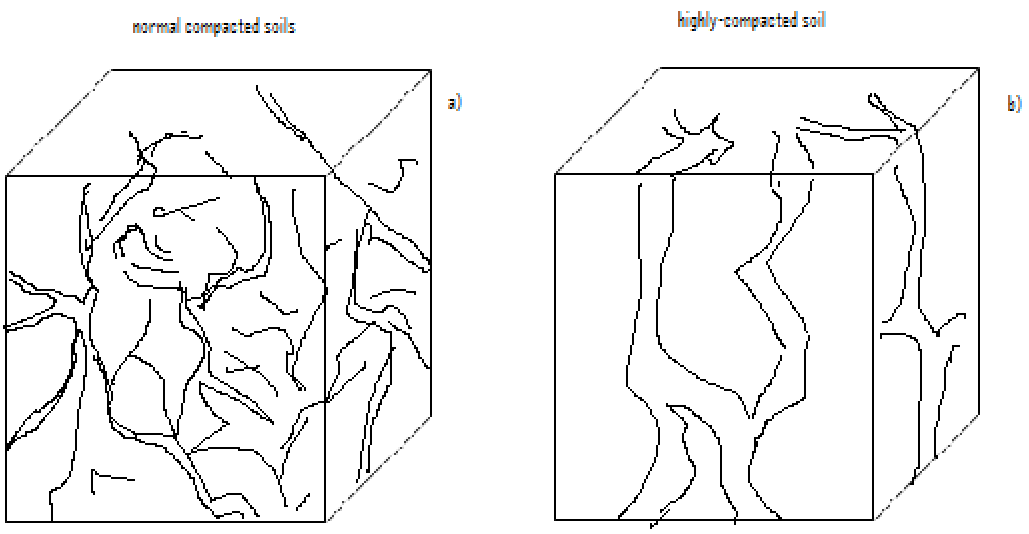

Figure 26 : Illustration showing two blocks of soils with different degree of compaction a) normally compacted soil with lower bulk density b) highly compacted soil with large macropores leading to high bulk density where the water transport is constrained within the persistent cracks.

5% arrival times are found positively correlated with air permeability *in-situ* and slightly correlated with *ka(-20).* It seems that the air transport is less sensitive to the pore size than the water transport since the viscosity of the fluid is playing an important role in velocity of fluid circulation through the pores.

It was not possible to link the 5% arrival times and tritium recovery rate with water transport from our leaching experiments because of the limited number of hydraulic conductivity measurements (Figure 16). However, we expect a negative correlation between log(*Ks*) and 5% tracer arrival times.

Apparent dispersivity in this study doesn't exactly reflect the hydrodynamic dispersivity from CDE equation. However, it still gives a relative value reflecting the spreading of the BTC. The contour map (Figure 20a) show the highest values of apparent dispersivity on the upper part and in the lower left corner, while the lowest values are found in the centre of the field. Apparent dispersivity is strongly correlated with 5% arrival times resulting from leaching experiment (Figure 27b). Small 5% arrival times imply high apparent dispersivity. Though when we plotted 5% arrival times from leaching experiment against the ones calculated from BTCs (Figure 27a), the strong correlation was found only for the column having a high percentage of tritium recovery. The prediction of 5% arrival time from BTC would be improved by extending the sampling time of experiment.

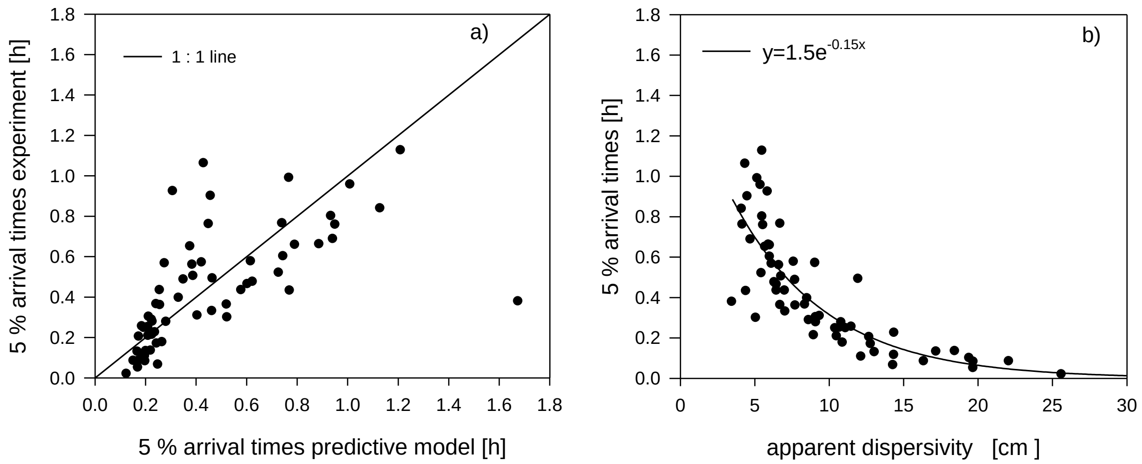

Figure 27 : a) the relation between 5% arrival times from leaching experiment and BTC; b) 5% arrival time as a function of apparent dispersivity

When looking at the contour maps of bulk density, 5% arrival times, tritium recovery and apparent dispersivity, we can see that the risk of macropore flow is mainly present in the third upper part and on the borders of the field where the field road is passing and the area is not ploughed. The centre of the field is ploughed regularly, thus promoting the matrix flow.

4.4.2 Suggested tool for predicting and mapping risk of macropore flow

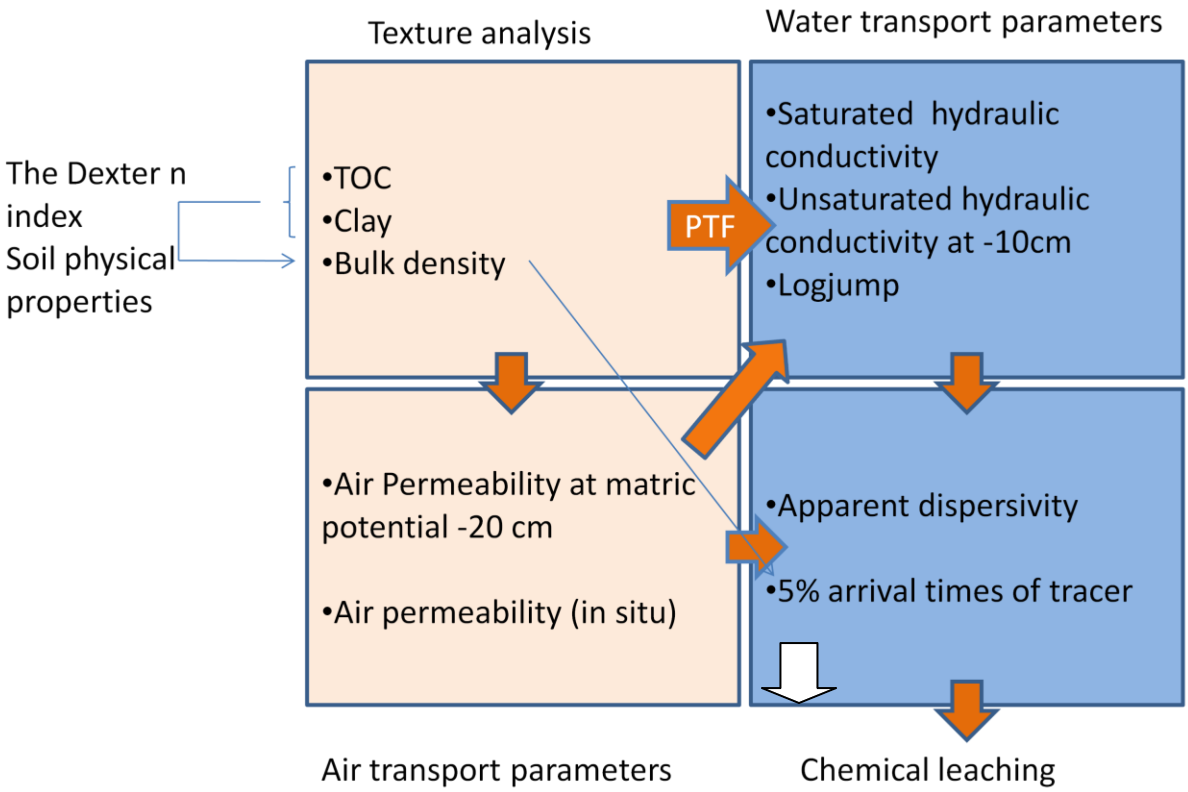

Figure 28 : The linkage between four different groups of functional soil parameters. These parameters linked by simple correlation or pedo-transfer-functions (PTFs) and combined with smart field-scale mapping of the parameters can become a new, valuable tool for assessment of chemical leaching risks. The combined mapping and PTF tool is suggested as a part of a decision platform for managing pesticide application at the field

The clay content and OC content are more or less directly influencing the fate of contaminants in soils. The pool of "hungry'' soils facilitates dispersion of clay in water , thus promoting the colloid facilitated transport in soils, while organic carbon plays an important role in retardation of various chemical compounds percolating with the soil solutions. Moreover, this two fundamental parameters together with other factors, such as soil management, climate conditions etc., strongly influence the structure of soils, the latter controlling the movement of contaminants through the macropores towards groundwater.

The fate of contaminants can be studied by many approaches depending on the goal and limitation of project. The laboratory tests, such as hydraulic conductivity and leaching experiments on the undisturbed soil columns can exactly describe the solute transport in soils but are very expensive and time consuming. The prediction of solute transport and fate of contaminants by means of soil texture analysis applying the pedo-transfer function or air permeability measurements is less expensive and easier but it must be used with thoughtfulness.

5 Conclusion

- The soil structure of Silstrup field is strongly heterogeneous, with higher macropore occurrence in the northern part and on the borders of the field.

- Air permeability *in situ* can be used for prediction of water transport.

- PTF is a useful tool for mapping the risk of macropore flow at large regional scale, though it should be used with thoughtfulness at field scale

- The prediction of macropore flow at field scale can be improved by reducing the grid of sampling.

- 5% arrival times may be used as a predictor to improve PTF.

- Double log normal model with more parameters performs better than log normal model when fitting the breakthroughs curve to the measured data

- The best correlation was obtained between the soil bulk density and 5% arrival times and tritium recovery in the effluent; this confirms the preferential water circulation through the macropores and influence of soil tillage on the soil structure.

- Organic carbon and clay content strongly influence the soil structure but are not directly correlated with 5% arrival time and apparent dispersivity – the parameters obtained from leaching experiments

- The laboratory tests, such as hydraulic conductivity and leaching experiments on the undisturbed soil columns can exactly describe the solute transport in soils but are very expensive and time consuming.

- The prediction of solute transport and fate of contaminants by means of soil texture analysis applying the pedo-transfer function or air permeability measurements is less expensive and easier but it must be used with thoughtfulness.

Reference

Aimrun, W., & Amin, M. S. M. (2009). Pedo-transfer function for saturated hydraulic conductivity of lowland paddy soils. Paddy and Water Environment, 7(3), 217-225. Springer Berlin / Heidelberg

Bouma, J. (1981). Soil morphology and preferential flow along macropores. Agricultural Water Management, 3(4), 235-250

Beven, K. and P. German. 1982. Macropores and water flow in soils. Water Resour. Res. 18(5):1311-1325.

Børgesen, C.D., B.V. Iversen, O.H. Jacobsen, and M.G. Schaap. 2008. Pedotransfer functions estimating soil hydraulic properties using different soil parameters. Hydrol. Process. 22(11):1630- 1639.

Børgesen, C.D., O.H. Jacobsen, S. Hansen, and M.G. Schaap. 2006. Soil hydraulic properties near saturation, an improved conductivity model. J. Hydrol. 324(1-4):40-50.

Cislerova, M., J. Simunek, and T. Vogel (1988). Changes of steady state infiltration rates in recurrent ponding infiltration experiments. Journal of Hydrology 104(1-4): 1-16.

de Jonge, L.W., P. Moldrup, G.H. Rubæk, K. Schelde, and J. Djurhuus. 2004. Particle leaching and particle-facilitated transport of phosphorus at field scale. Vadose Zone J. 3(2):462-470.

de Jonge, L.W., P. Moldrup, H. de Jonge, and R. Celis. 2008. Sorption and leaching of shortterm-aged PAHs in eight European Soils: Link to physico-chemical properties and leaching of dissolved organic carbon. Soil Sci. 173: 13-24

de Jonge L. W., P. Moldrup, and P. Schjønning. 2009. Soil Infrastructure, Interfaces and transocation processes in inner space (“soil-it-is”): towards a raod map for the constraints and crossroads of soil architecture and biophysical processes. Hydrol. Earth Syst. Sci. Discuss., 6, 2633–2678

Demuth, H., and M. Beale, 2000. Neural Network Toolbox. The Mathworks, Natick, Massachusetts, USA.

Dexter, A. R., Richard, G., Arrouays, D., Czyz, E. A., Jolivet, C., and Duval, O. 2008. : Complexed Organic matter controls soil physical properties, Geoderma, 144, 620–627

Doerr, S. H., R. A. Shakesby, and R. P. D. Walsh (2000). Soil water repellency: Its causes, characteristics and hydro-geomorphological significance. Earth-Science Reviews 51(1-4): 33-65.

Jarvis, N.J. 2007. A review of non-equilibrium water flow and solute transport in soil macropores: principles, controlling factors and consequences for water quality. Eur. J. Soil Sci. 58(3):523-546.

Jury, W. A. (1982). Simulation of solute transport using a transfer-function model. Water Resources Research 18(2): 363-368.

Jury, W. A. and K. Roth (1990). Transfer functions and solute movement through soil: Theory and applications. Basel, Switzerland, Birkhauser Verlag AG.

Jury, W. A. and G. Sposito (1985). Field calibration and validation of solute transport models for the unsaturated zone. Soil Science Society of America Journal 49(6): 1331-1341.

GEUS The Danish Pesticide Leaching Assessment Programme,2000, 2009

Gee G.W & Or. D., 2002. Methods of soils Analysis part 4-physical methods. Book series No. 5. Edt. By Dane, J.H. and Topp, G.C. Madison, Wisconsin, USA. Soils Science Society of America.

Greve, M.H., M.B. Greve, P.K. Bøcher, T. Balstrom, H. Breuning-Madsen, and L. Krogh. 2007.

Hendrickx, J. M. H. and M. Flury (2001). Uniform and preferential flow mechanisms in the vadose zone. Conceptual models of flow and transport in the fractured vadose zone: 149-187.

Hillel, D. 1998. Environmental Soil Physics, London, Academic Press, 1998. 771 pp..

Klute, A. 1986. Water retention: Laboratory methods. p. 635–662. In A. Klute (ed.) Methods of soil analysis, Part 1. Physical and mineralogical methods. ASA and SSSA, Madison, WI.

Klute, A., and C. Dirksen. 1986. Hydraulic conductivity and diffusivity: Laboratory methods. p.687–734. In A. Klute (ed.) Methods of soil analysis, Part 1. Physical and mineralogical methods. ASA and SSSA, Madison, WI.

Knudby, C. and J. Carrera (2005). On the relationship between indicators of geostatistical, flow andtransport connectivity. Advances in Water Resources 28(4): 405-421.

Lindhardt, B. Abildtrup, C., Vosgerau, H., Olsen,P., Torp, S., Iversen, B. V., Jørgensen, J.O., Plauborg, F., Rasmussen,P., Gravesen, P.,2001. The Danish Pesticide Leaching Assessment Programme-Site Characterization and Monitoring Design. Geological Survey of Denmark and Greenland.

Loll, P. Moldrup, P.,2000. Soil Characterization and Polluted soils Assessment. Aalborg University

Mualem, Y. 1976. A new model for predicting the hydrologic conductivity of unsaturated porous media. Water Resour. Res. 12:513-522.

Nemes, A., Rawls, W. J., & Pachepsky, Y. A. (2005). Influence of organic matter on the estimation of saturated hydraulic conductivity. Soil Science Society of America Journal, 69(4), 1330-1337.

Raats, P. A. C. (1973). Unstable wetting fronts in uniform and nonuniform soils. Soil Science Society of America Journal 37(5): 681-685.

Rawls, W Effect of soil organic carbon on soil water retention Geoderma 2003 116 1-2 61-76

Schaap, M.G., and W. Bouten. 1996. Modelling water retention curves of sandy soils using neural networks. Water Resour. Res. 32:3033– 3040.

Schaap, M.G., and F.L. Leij. 1998. Using neural networks to predict soil water retention and soil hydraulic conductivity. Soil Till. Res. 47:37–42.

Schjønning, P. 1985. Equipment for drainage of soil samples (in Danish with English abstract). Tidsskrift for Planteavls Specialserie. København: Statens Planteavlsforsøg. Beretning nr. S 1762:1- 520 25.

Schjønning. P., and K. J. Rasmussen. 1989. Long-Term Reduced Cultivation. I. Soil Strength and Stability. Soil Till. Res. 15(1-2):79-90.

Skaggs, T. H., Z. J. Kabala, and W. A. Jury (1998). Deconvolution of a nonparametric transfer function for solute transport in soils. Journal of Hydrology 207(3-4): 170-178.

Snehota, M., M. Sobotkova, and M. Cislerova (2008). Imapct of the entrapped air on water and solute transport in an heterogeneous soil: experimental setup. Journal of Hydrology and Hydromechanics 56(4): 247-256.

Stagnitti, F., G. Allinson, M. Morita, M. Nishikawa, H. Ii, and T. Hirata (2000). Temporal moments analysis of preferential solute transport in soils. Environmental Modeling & Assessment 5(4): 229-236.

Sukhija, B. S., Reddy, D. V., Nagabhushanam, P., & Hussain, S. (2003). Recharge processes: piston flow vs preferential flow in semi-arid aquifers of India. Hydrogeology Journal, 11(3), 387-395

Trine Nørgaard, Master thesis Aalborg university 2011

Ulén, B., and K. Persson. 1999. Field-scale phosphorus losses from a drained clay soil in Sweden. Hydrol. Process. 13(17):2801-2812.

Utermann, J., E. J. Kladivko, and W. A. Jury (1990). Evaluating pesticide migration in tile-drained soils with a transfer-function model. Journal of Environmental Quality 19(4): 707-714

Van den Elsen, E., J. Stolte, and G. Veerman. 1999. Three automated laboratory systems for determining the hydraulic properties of soils. pp. 329-340. In Characterization and Measurement of the Hydraulic Properties of Unsaturated Porous Media, Part 1.

Van Genuchten, M.T. 1980. A closed-form equation for predicting the hydraulic conductivity of unsaturated soils. Soil Sci. Soc. Am. J. 44:892-898.

Vanderborght, J. and H. Vereecken (2007). Review of dispersivities for transport modeling in soils.Vadose Zone Journal 6(1): 29-52.

Column no.	Clay (<2 µm)	Silt (2-20µm)	Coarse silt (20-50 µm)	Fine sand (50-63 µm)	Fine sand (63-125 µm)	Fine sand (125-200 µm)	Coarse sand (200-500 µm)	Coarse sand (500-2000 µm)	Humus	$CaCO_3$	Total C
	g/100 g	g/100 g	g/100 g	g/100 g	g/100 g	g/100 g	g/100 g	g/100 g	g/100 g	g/100 g	g/100 g
1	**14,8**	15,9	14,5	4,6	14,5	9,4	15,8	7,1	3,5	-1	2,05
2	14,9	15,8	13,9	5,5	14,9	8,8	16,4	6,4	3,4	-1	2,02
3	14,2	16,5	13,8	4,9	15,6	9,0	16,4	6,2	3,5	-1	2,06
4	14,3	17,1	13,8	4,7	15,4	8,9	15,9	6,5	3,5	-1	2,03
5	14,2	17,2	13,2	4,2	14,9	9,6	16,8	6,5	3,4	-1	2,01
6	14,9	16,5	14,4	5,3	14,4	8,1	15,9	7,1	3,5	-1	2,03
7	14,9	16,5	14,5	4,8	14,9	9,0	15,8	6,1	3,4	-1	2,02
8	14,3	17,1	14,1	5,2	14,9	8,9	16,0	6,1	3,4	-1	2,00
9	14,9	16,5	12,3	7,1	14,8	9,5	16,0	5,5	3,6	-1	2,11
10	15,0	16,4	14,0	4,8	14,3	9,0	16,7	6,6	3,4	-1	2,00
11	15,0	15,7	15,8	4,2	15,0	9,7	15,9	5,3	3,5	-1	2,03
12	15,1	16,3	13,1	6,5	14,7	8,1	15,8	7,0	3,4	-1	2,02
13	15,4	15,9	14,7	5,1	15,3	8,8	15,6	5,7	3,4	-1	1,99
14	15,6	16,4	14,6	4,9	14,2	7,9	16,1	6,9	3,4	-1	2,02
15	15,0	15,7	12,3	7,2	15,0	9,2	15,9	6,2	3,6	-1	2,09
16	15,0	16,4	15,1	4,7	13,8	7,9	17,0	6,6	3,6	-1	2,11
17	14,3	17,1	16,3	5,7	13,7	8,8	15,5	5,3	3,5	-1	2,04
18	14,4	16,3	12,8	7,2	15,1	8,8	16,1	5,8	3,5	-1	2,07
19	14,3	16,4	15,8	4,8	15,9	8,8	15,1	5,8	3,2	-1	1,90
20	14,3	16,4	12,9	6,7	14,6	9,0	15,8	7,0	3,2	-1	1,90
21	14,4	17,0	14,6	4,9	15,1	8,6	16,5	5,5	3,5	-1	2,03
22	14,3	16,4	12,9	7,4	14,0	9,5	15,4	6,7	3,4	-1	1,98
23	14,4	17,6	14,6	4,8	15,4	8,7	15,7	5,5	3,3	-1	1,94
24	15,0	17,0	11,8	7,5	15,1	9,0	15,6	5,8	3,3	-1	1,92
25	15,0	17,0	14,8	4,9	14,6	8,4	15,3	6,8	3,3	-1	1,91
26	14,4	17,0	12,7	7,1	14,9	9,0	15,9	5,5	3,6	-1	2,13
27	14,3	17,1	14,5	5,4	14,9	9,3	15,7	5,5	3,4	-1	1,98
28	15,0	16,4	14,4	6,0	14,3	9,1	16,2	5,2	3,5	-1	2,07
29	16,2	15,8	13,3	6,0	15,1	8,4	15,8	6,0	3,4	-1	2,01
30	15,4	15,2	15,7	4,2	15,3	8,7	16,5	5,7	3,3	-1	1,91
31	16,9	15,1	13,9	6,9	14,4	8,8	15,0	5,3	3,7	-1	2,16

32	16,9	17,1	14,4	4,6	16,1	8,5	14,4	4,4	3,7	-1	2,20
33	16,1	16,6	11,6	7,5	14,6	9,2	15,3	5,7	3,5	-1	2,08
34	16,1	16,6	13,4	5,3	14,6	9,0	15,6	6,0	3,4	-1	1,98
35	16,1	16,6	13,2	6,9	14,7	8,7	14,9	5,6	3,3	-1	1,95
36	18,9	17,7	14,7	4,8	14,1	7,5	13,4	5,2	3,7	-1	2,17
37	17,6	17,8	12,5	6,7	13,6	8,2	13,9	6,1	3,6	-1	2,11
38	16,8	17,2	14,7	4,1	14,7	7,7	15,9	5,6	3,3	-1	1,96
39	16,1	16,6	13,3	6,9	14,9	8,8	14,6	5,6	3,2	-1	1,89
40	16,7	16,0	14,0	4,6	16,3	8,2	14,6	6,1	3,5	-1	2,08
41	18,9	17,7	14,8	4,1	13,4	8,2	13,1	6,6	3,3	-1	1,91
42	18,3	16,4	12,6	6,9	13,5	8,4	14,2	6,7	3,1	-1	1,83
43	17,6	17,1	14,8	4,8	14,3	7,7	13,7	6,6	3,4	-1	2,01
44	17,0	16,3	12,6	7,7	14,6	8,7	14,4	5,4	3,4	-1	1,98
45	16,2	16,4	13,5	6,2	14,9	8,2	14,4	7,1	3,1	-1	1,81
46	16,9	16,4	15,1	5,0	14,2	8,1	14,3	6,8	3,1	-1	1,83
47	16,9	16,4	12,4	6,2	13,9	9,8	15,2	6,0	3,1	-1	1,82
48	17,0	17,7	14,2	5,3	14,5	8,1	14,0	5,8	3,5	-1	2,05
49	16,2	16,4	12,6	7,1	14,6	8,7	14,4	6,6	3,3	-1	1,96
50	16,8	15,9	13,8	4,7	15,2	8,6	14,8	7,4	2,9	-1	1,70
51	18,5	18,2	12,2	7,2	13,6	8,1	13,4	5,9	3,0	-1	1,77
52	14,6	20,8	11,3	4,7	14,8	8,8	14,7	7,4	3,0	-1	1,75
53	16,1	15,2	13,5	6,2	14,2	8,3	14,5	8,8	3,2	-1	1,89
54	16,2	16,4	11,4	6,8	14,2	9,2	15,3	7,2	3,3	-1	1,94
55	16,9	16,4	13,0	4,6	14,2	8,5	15,4	8,0	3,0	-1	1,75
56	18,9	17,7	12,1	6,4	13,3	7,5	12,9	7,9	3,2	-1	1,87
57	16,8	16,5	13,3	4,7	13,8	7,8	15,0	8,9	3,1	-1	1,82
58	14,6	14,1	9,2	5,7	13,2	8,1	18,5	13,5	3,1	-1	1,84
59	16,6	14,1	11,8	6,4	14,2	8,8	16,5	8,2	3,3	-1	1,95
60	17,5	15,2	13,1	4,8	14,3	8,4	15,7	8,2	2,9	-1	1,71
73	15,6	16,4	11,6	7,4	14,1	9,1	15,8	6,5	3,5	-1	2,06
74	15,5	15,8	14,8	5,3	14,9	8,6	15,6	6,2	3,3	-1	1,93
75	17,6	17,1	14,3	5,2	14,1	7,3	14,7	6,4	3,3	-1	1,94
76	16,2	16,4	11,6	6,5	14,1	9,5	15,7	6,7	3,1	-1	1,81
77	16,2	16,4	12,4	4,8	14,1	8,8	16,0	8,5	2,9	-1	1,73

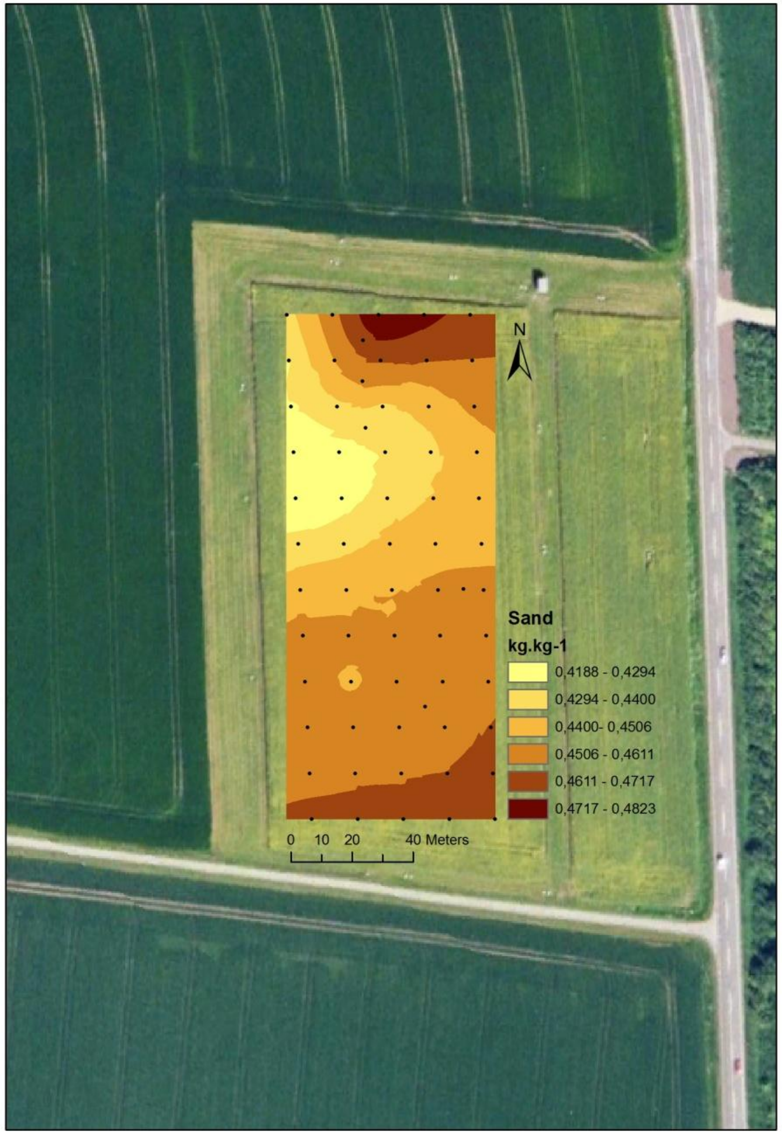
N
Sand
kg.kg-1
0,4188 - 0,4294
0,4294 - 0,4400
0,4400- 0,4506
0,4506 - 0,4611
0,4611 - 0,4717
0,4717 - 0,4823
0 10 20 40 Meters

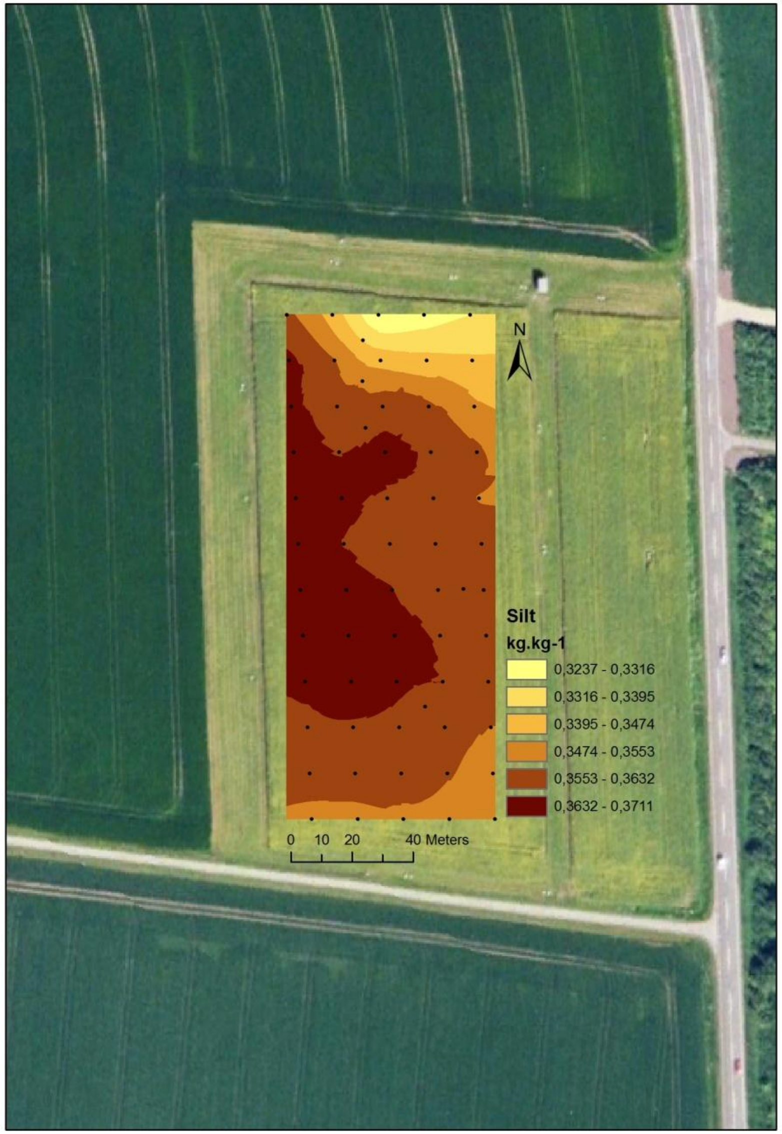
N
Silt
kg.kg-1
0,3237 - 0,3316
0,3316 - 0,3395
0,3395 - 0,3474
0,3474 - 0,3553
0,3553 - 0,3632
0,3632 - 0,3711
0 10 20 40 Meters

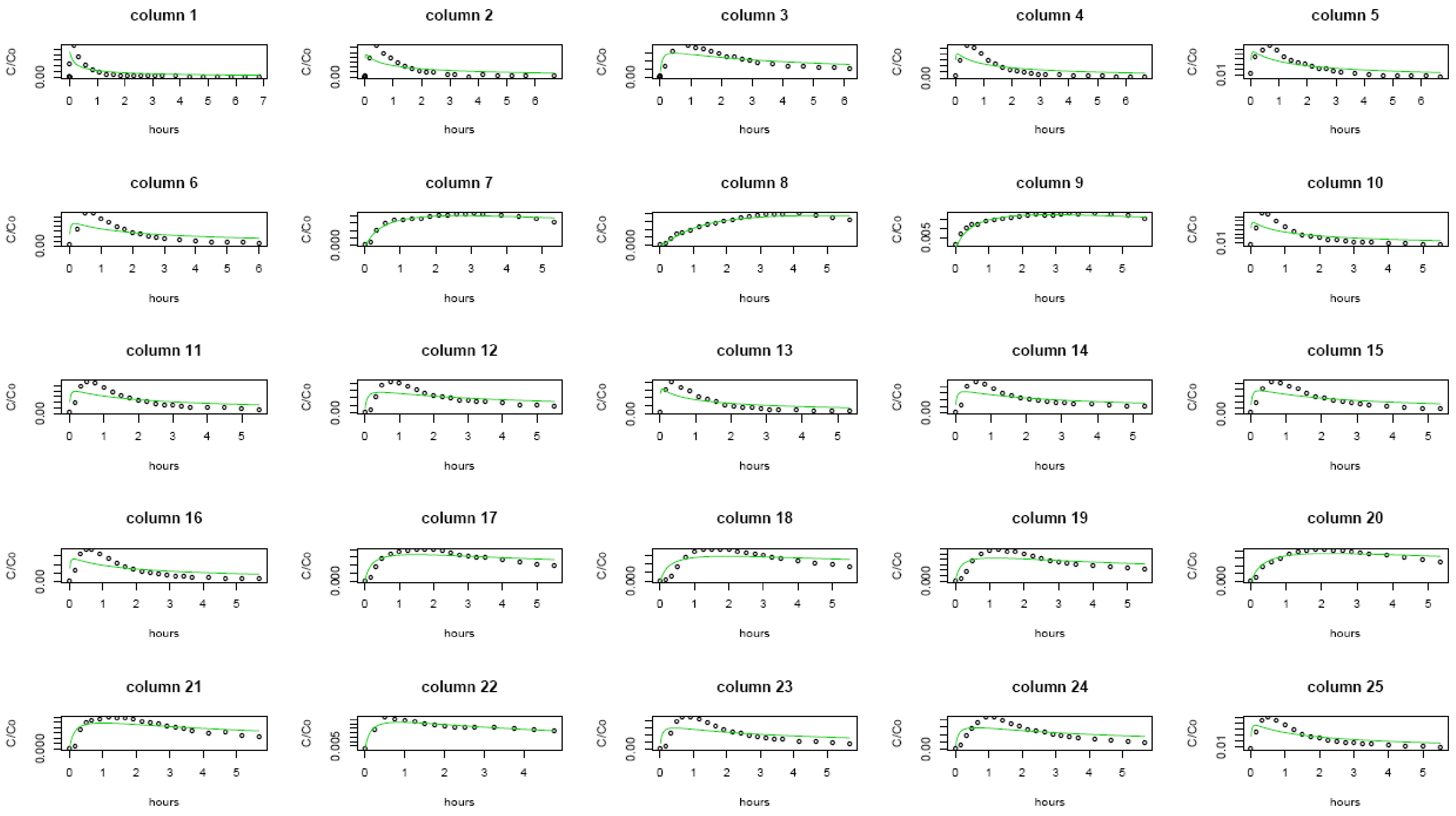
column 1
column 2
column 3
column 4
column 5
column 6
column 7
column 8
column 9
column 10
column 11
column 12
column 13
column 14
column 15
column 16
column 17
column 18
column 19
column 20
column 21
column 22
column 23
column 24
column 25
C/Co
hours

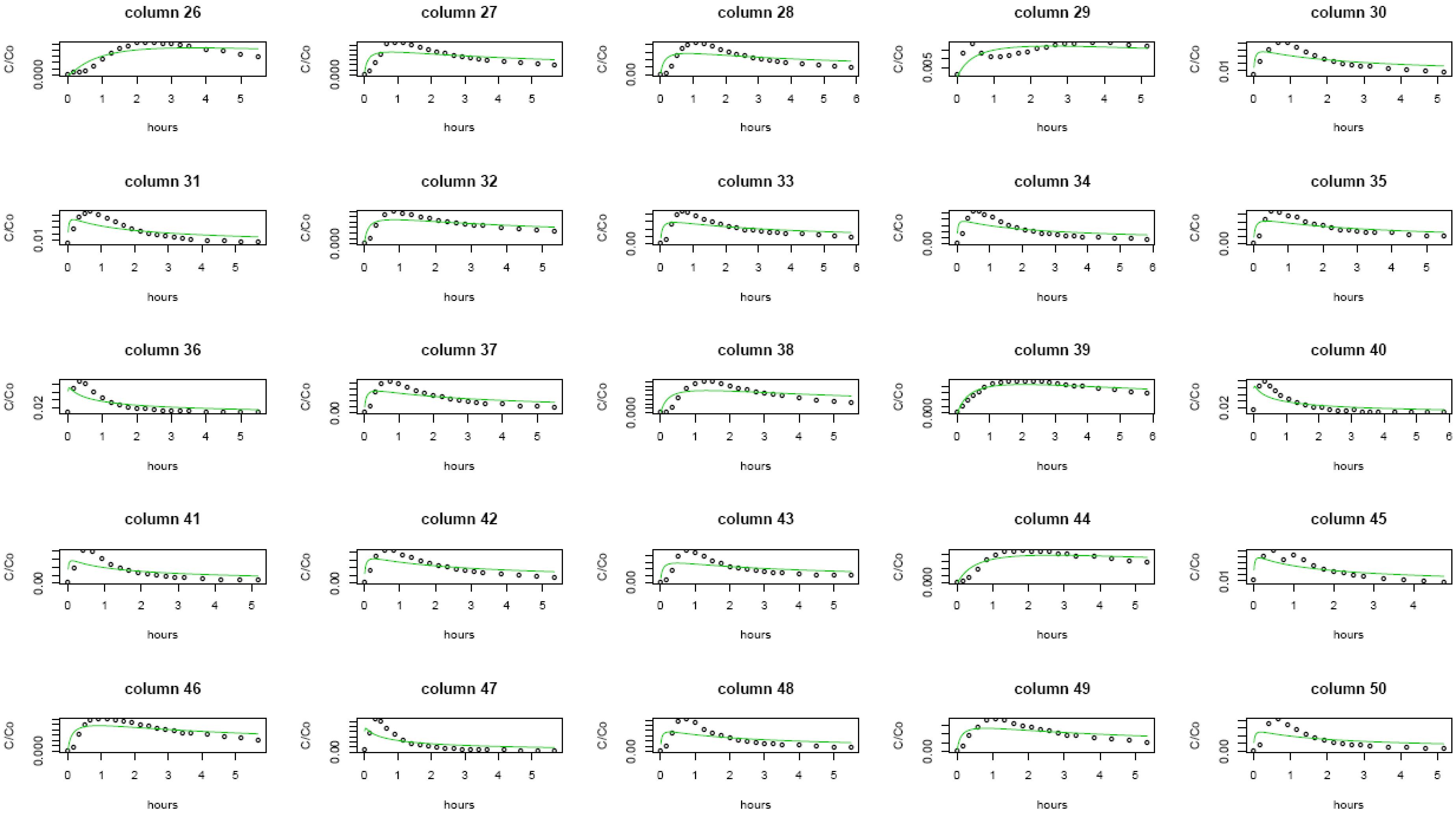
column 26
column 27
column 28
column 29
column 30
column 31
column 32
column 33
column 34
column 35
column 36
column 37
column 38
column 39
column 40
column 41
column 42
column 43
column 44
column 45
column 46
column 47
column 48
column 49
column 50
C/Co
hours

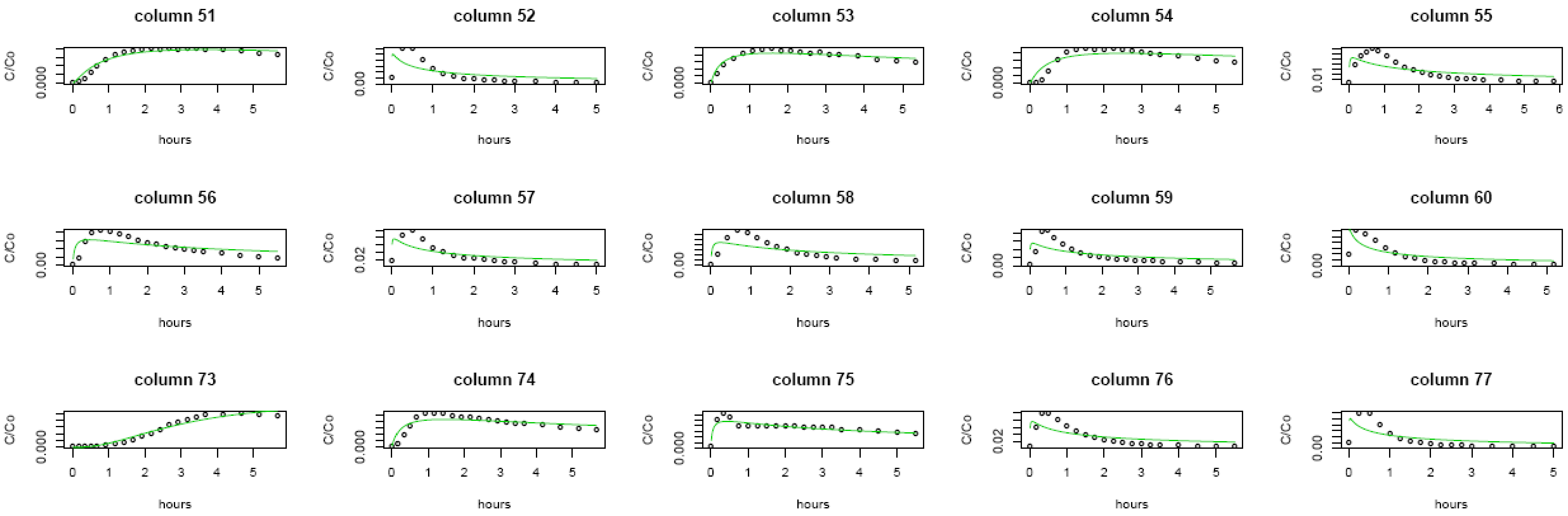
column 51
column 52
column 53
column 54
column 55
column 56
column 57
column 58
column 59
column 60
column 73
column 74
column 75
column 76
column 77
C/Co
hours

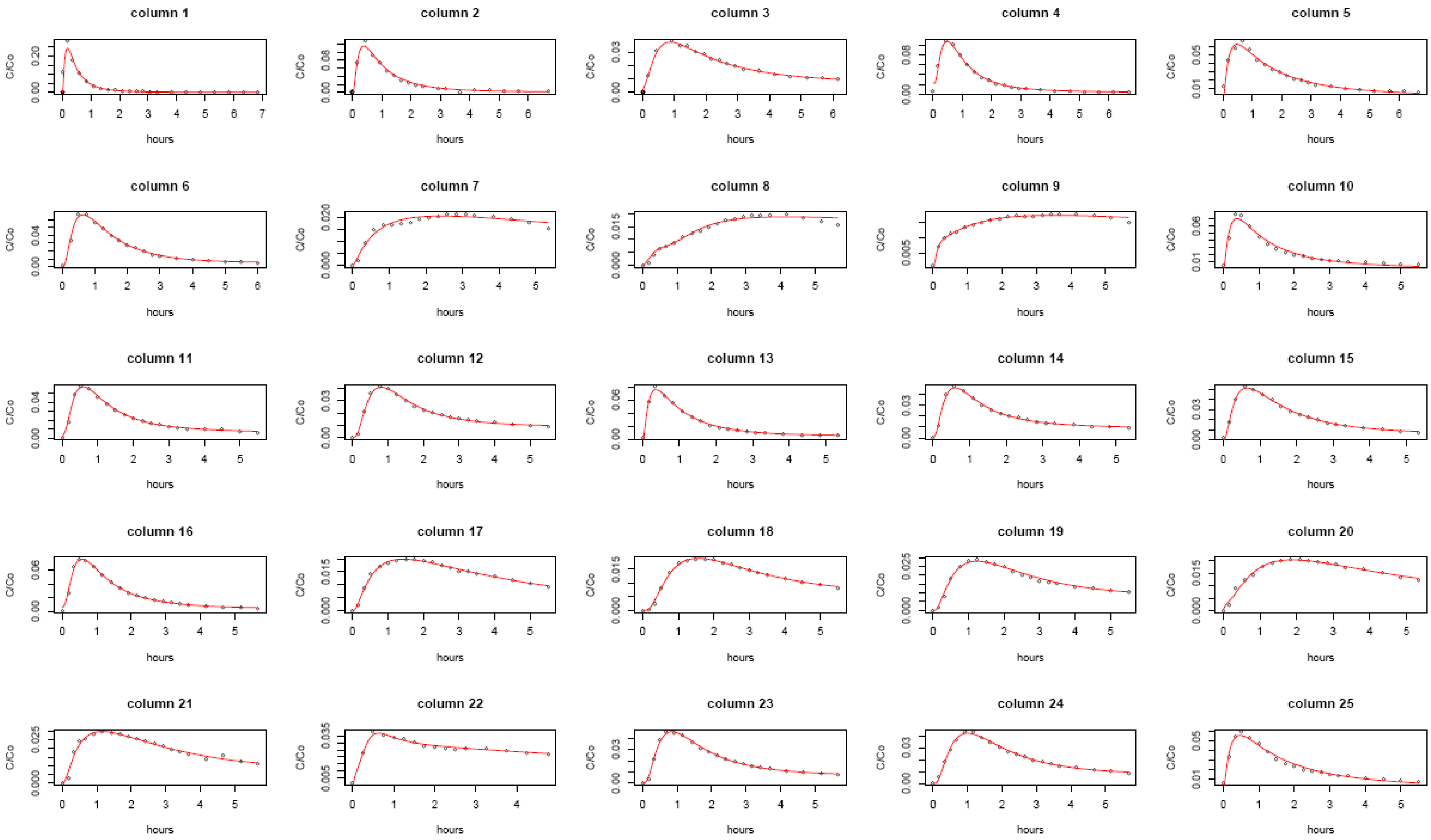
column 1
column 2
column 3
column 4
column 5
column 6
column 7
column 8
column 9
column 10
column 11
column 12
column 13
column 14
column 15
column 16
column 17
column 18
column 19
column 20
column 21
column 22
column 23
column 24
column 25
C/Co
hours

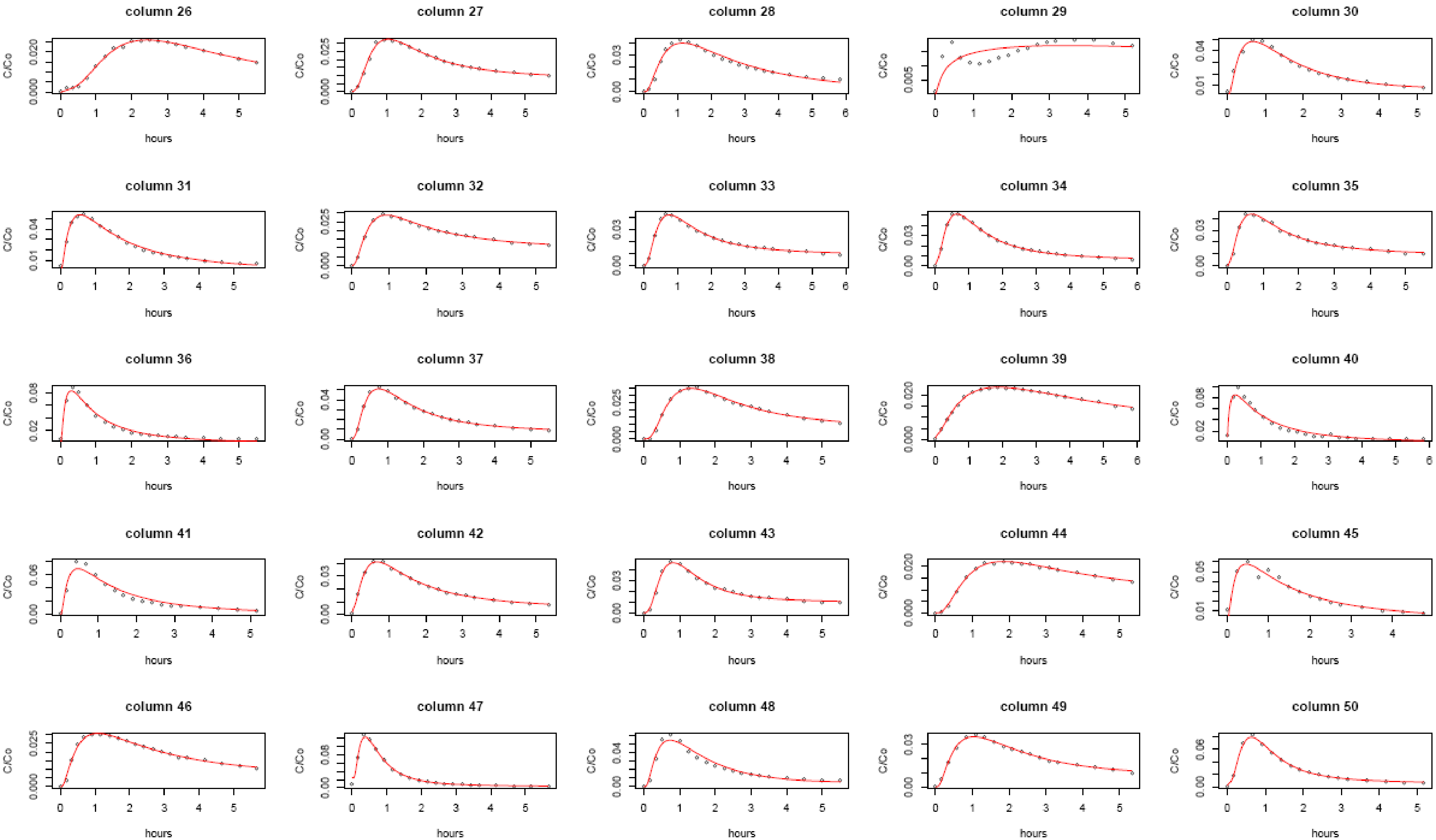
column 26
C/Co
hours
column 27
C/Co
hours
column 28
C/Co
hours
column 29
C/Co
hours
column 30
C/Co
hours
column 31
C/Co
hours
column 32
C/Co
hours
column 33
C/Co
hours
column 34
C/Co
hours
column 35
C/Co
hours
column 36
C/Co
hours
column 37
C/Co
hours
column 38
C/Co
hours
column 39
C/Co
hours
column 40
C/Co
hours
column 41
C/Co
hours
column 42
C/Co
hours
column 43
C/Co
hours
column 44
C/Co
hours
column 45
C/Co
hours
column 46
C/Co
hours
column 47
C/Co
hours
column 48
C/Co
hours
column 49
C/Co
hours
column 50
C/Co
hours

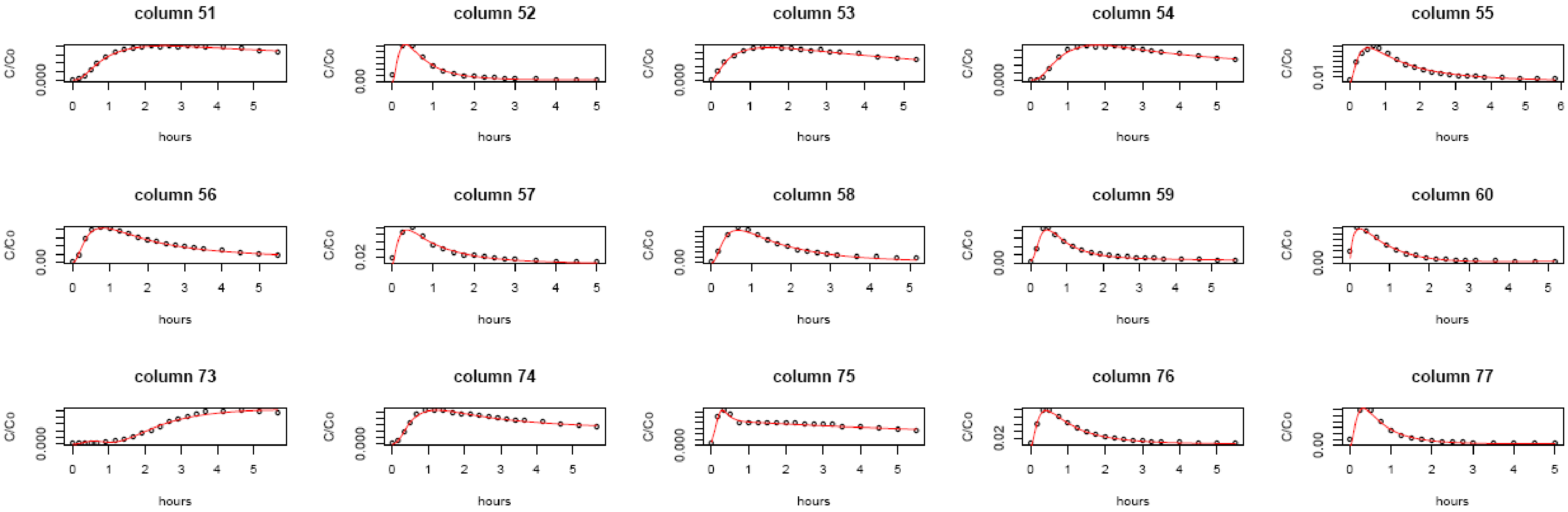
column 51
column 52
column 53
column 54
column 55
column 56
column 57
column 58
column 59
column 60
column 73
column 74
column 75
column 76
column 77
C/Co
hours